CAVITATION EROSION OF WC-Co

by

S. E. Hankey

A thesis submitted to the Faculty of Engineering, University of Cape Town in fulfillment of the degree of Master of Science in Applied Science

Department of Materials Engineering
University of Cape Town

September 1987

ABSTRACT

An investigation involving the vibratory cavitation erosion of WC-Co alloys was undertaken in order to determine the mechanisms of material removal.

Nineteen grades of WC-Co alloys were studied. These alloys had been previously characterised according to microstructural and mechanical properties. Further characterisation by way of Youngs modulus and density of the materials was undertaken.

An investigation of the influence of various parameters on cavitation erosion established a binder content dependence on erosion. For two grain sizes, erosion was found to increase to a maximum at 12 vol-% binder content (1.8 μm grain size) and 23 vol-% binder (2.8 μm grain size).

The main mode of material removal was found to be cobalt removal followed by WC grain pull-out. In high binder content alloys, cobalt removal was predominant with little loss of WC grains. X-ray diffraction showed that the allotropic phase transformation of the binder under cavitational attack was beneficial to the erosion resistance of these alloys. The erosion of low binder content alloys was controlled by the contiguity of the WC skeleton. Maximum erosion occurred at binder contents which corresponded to the combination of a fragile WC skeleton and a small volume of available cobalt for strain induced transformation.

ACKNOWLEDGEMENTS

I would like to thank the following people who assisted me in producing this thesis:

Professor A. Ball, my supervisor, for his help and advice.

Mr N. Dreze and Mr G. Newins for their technical assistance.

Mr B. Greeves for the photographic work.

Miss C. Lang, Mrs S. Betz and Mrs H. Bohm for their help in preparing the manuscript.

Staff and fellow students for their support and encouragement.

CONTENTS

CHAPTER 1

INTRODUCTION

Cavitation was first recognised as a cause of erosion over a century ago. The incidence of cavitation erosion in hydraulic systems is a long standing problem which is increasing due to higher operational pressures and speeds.

Heathcock (16) conducted a study of the cavitation erosion of a large variety of alloys and polymers in an attempt to determine the metallurgical variables which control erosion resistance. Although the most convenient criteria for predicting erosion resistance of materials are the readily available mechanical properties, it is now understood (32,33) that erosion is controlled by the material microstructure and not necessarily the bulk mechanical properties.

During the course of the study, Heathcock (16) found that the erosion resistance of nickel based cemented carbides was comparable with that of Stellites. WC-Co alloys did not perform as well as the WC-Ni alloys. This was surprising in view of the better properties of cobalt as a binder. The WC-Co alloys did not display the expected decrease in erosion with increasing hardness, as shown by the nickel based alloys. Instead a minimum in erosion was found at 15 wt-% cobalt. Heathcock proposed that this minimum was a result of the allotropic phase transformation of the binder from the metastable face centred cubic form to the hexagonal close packed form. The transformation was presumed to be detrimental to the erosion resistance of the WC-Co alloys. The volume reduction associated with the transformation increases the tensile stresses across the matrix-carbide interface which, it was proposed, could lead to debonding of the matrix. This effect would overshadow any increase in erosion resistance due to increasing hardness as the binder content is reduced below 15 wt-% cobalt.

This study was undertaken to determine a mechanism of cavitation erosion of WC-Co alloys and the effect of microstructure thereon. The alloys used in this investigation had been previously microstructurally characterised by Pennefather (28). The objectives of the study were to:

1. Further characterise the materials by determination of the Youngs modulus and the binder content of the alloys.

2. To determine the influence of various microstructural parameters on the cavitation erosion of WC-Co alloys using a vibratory cavitation erosion rig. The cavitation parameters used were the same as used previously by Heathcock.

3. To determine a mechanism of material removal during cavitation erosion by examination of the eroded surfaces during the incubation time and the steady state erosion region.

4. To determine the transformation of the binder during cavitation erosion using X-ray diffraction and its effect on the erosion resistance of the alloys.

5. To monitor the possible synergistic effect of corrosion on the erosion of the alloys.

CHAPTER 2

CAVITATION EROSION

Cavitation, often defined as the formation, growth and collapse of vapour bubbles due to local pressure fluctuations, is known to occur in many hydrodynamic engineering situations (18).

If the pressure of a body of liquid is reduced at constant temperature by dynamic means to below the vapour pressure, the tensile stress imposed in the liquid generates cavities. If a growing bubble is subjected to a pressure increase, its growth will be arrested and reversed. These cavities then collapse violently, each bubble emitting a pressure wave of order of magnitude 1000 MPa into the surrounding liquid (40). This wave is rapidly attenuated with distance, but those bubbles collapsing close to a solid surface will be capable of damaging that surface.

In short, cavitation is:

- a liquid phenomenon and does not occur under normal circumstances in either solid or gas
- the result of pressure fluctuations in a liquid
- concerned with the appearance and disappearance of cavities in a liquid
- a dynamic phenomenon.

2.1 EFFECTS OF CAVITATION

Cavitation can both modify the hydrodynamics of flow of the liquid and cause damage to solid-boundary surfaces of a system.

Uncontrolled cavitation can lead to serious erosion or catastrophic results. Susceptible equipment or structures include: all types of turbines, centrifugal and axial flow pumps, pipelines, propellors, rudders and even the hulls of ships. Cavitation may be aggravated by poor design but may occur in the best designed equipment under unfavourable conditions (19).

Cavitation erosion damage involves the removal of material from the surface of solid flow boundaries. All materials are susceptible in varying degrees to cavitation damage: cavitation is basically a mechanical/fluid dynamics

problem, not a material problem. The inception of cavities and subsequent intensity of cavitation is little influenced by particular construction materials of the system. The resultant erosion damage to the material, however, is a function of the composition, microstructure and mechanical characteristics of the material.

2.2 VIBRATORY CAVITATION

There are four kinds of cavitation, viz. travelling, fixed, vortex and vibratory, which are determined by the conditions and principal physical characteristics.

Vibratory cavitation is cavitation without major flow. In the other three types of cavitation, the liquid element passes through the cavitation zone only once. Here the forces causing cavities to form and collapse are due to a continuous series of high amplitude, high frequency pressure pulsations in the liquid.

Vibratory cavitation is generated by a submerged surface which vibrates normal to its face and sets up pressure waves in the liquid. The amplitude of the pressure wave must be great enough to cause the pressure to drop to or below the vapour pressure of the liquid.

The vibrating surface can be either one which vibrates unintentionally, e.g. a secondary effect from machine operation, or a device e.g. transducer designed for the specific purpose of producing a wave train in a liquid. The shape of the vibrating surface determines the type of wave train produced e.g. plane or diffused (minimum pressure at focal point within the body of the liquid).

2.3 MECHANISMS OF CAVITATION EROSION

The growth and collapse of bubbles generates stress pulses which are directed towards the walls. Rapid attenuation of the pulse means that to cause damage, a bubble must be less than its maximum radius from the surface. A bubble collapsing close to the surface suffers from geometrical constraints and becomes involuted, forming a jet of liquid which impacts the solid (32). This is thought to play only a minor role in erosion, as the major part of erosion by cavitation in a vibratory system results from

the integrated effect of a whole cloud of bubbles (40). This is because a cloud of bubbles collapsing in concert will create combined wave damages at greater distances.

Some pulses are great enough to cause plastic deformation of the surface and crater formation. In other cases, pulses promote the accumulation of fatigue-like hardening as a result of increased dislocation density. As hardening continues, local internal stresses increase until they are high enough to initiate fracture and material removal i.e. erosion (18).

Proposed mechanisms of material removal have been:

1. Accelerated Corrosion

   Preece (32) and Karimi and Martin (18) consider that cavitation damage accelerates corrosion by enhancing the dissolution of alloys which corrode in aqueous fluids. This leads to increased material loss. Knapp et al (19) suggest that if corrosive action results in a series of corrosion pits on the surface, they may act as wave guides. Wave guides act by concentrating the mechanical blows of the collapsing cavities and thus accelerating the damage. Vibratory tests, however, are generally "accelerated" compared with flow and field tests. The high intensity cavitation emphasizes the mechanical component, reducing the proportionate effect of corrosion. Thus this mechanism is not likely in vibratory cavitation (32, 19).

2. Localised Melting

   Vyas and Preece (39) disproved this possibility by observation of dislocations and surface slip lines in eroded aluminium using transmission electron microscopy (TEM). These defects would be removed by surface temperatures corresponding to the melting point of aluminium.

3. Mechanical Stressing

   The pulsatory, high amplitude stress resulting from imploding cavities may promote fatigue-like hardening of the superficial layers of the material, which increases the dislocation density (18).

This hardening increases with each pulse and eventually the internal stress may become enough to initiate fracture and material removal. Plesset and Ellis (31) found that polycrystalline and monocrystalline specimens exposed to cavitation undergo either eventual or almost immediate plastic deformation, depending on the hardness and yield properties of the material. This plastic deformation is essentially cold working of the material and leads to fatigue and failure of portions of the specimen. Vyas and Preece (40), using an X-ray technique for determining residual stress, found that the depth of the work hardened layer in nickel extended to a considerable depth and increased in depth with exposure time.

2.4 PREDICTION OF MATERIAL PERFORMANCE AND MATERIAL RESPONSE

A number of previous investigations have attempted to develop a means of predicting material performance under cavitation erosion. The most convenient criteria for such a prediction are macroscopic mechanical properties. For small groups of materials, such as alloys with a common base-metal, a good correlation between erosion resistance and properties such as hardness, yield strength and tensile strength has been found, but this is not true for a large range of materials. Other parameters which have been considered are Hobbs' ultimate resilience and strain energy to fracture.

It has been shown that erosion is controlled by the microstructure of the material and not necessarily by the bulk properties (33). Vaidya and Preece (37) found that the degree and depth of deformation, and the mode or rate of subsequent material removal is essentially determined by the ability of the material to absorb and dissipate cavitation energy.

Rao and Buckley (34) observed twins in materials which had been exposed to cavitation, which suggests that stacking faults are generated during cavitation attack. As the stacking fault energy (SFE) affects the microstructure, mode of deformation and fracture of a material, it is expected that materials with high SFE will erode faster under cavitation attack. Higher erosion resistance has been related to low stacking fault energy, which enables planar slip, higher work hardenability and phase transformation. These absorb some of the cavitation energy and are thus beneficial to erosion resistance (18).

The relatively high erosion resistance of cobalt alloys and austenitic alloys has been attributed to the phase transformation that occurs during cavitation erosion testing (41). Two reasons for the improvement of erosion resistance by phase transformation could be:

1. Phase transformations continuously absorb a portion of the cavitation energy, thus reducing the amount available for deformation and erosion.

2. Transformation produces a finely dispersed second phase which has essentially the same properties as the matrix. This effectively "subdivides" the grains into fine units, reducing the effective "grain size" and associated dislocation mean free path. This improves the erosion resistance (32).

In the case of cobalt based cemented carbides, however, Heathcock (16) proposed that the fcc → hcp phase transition of the binder has a detrimental effect on the erosion resistance. The reduction in volume associated with the transformation increases the tensile stresses across the cobalt-carbide interface, which may result in debonding between the matrix and binder phases, and hence increased erosion.

In general, Preece (32) found that a fine grain size combined with a ductile mode of erosion was beneficial to erosion resistance. Heathcock (16), after studying a wide range of materials, proposed that a cavitation erosion resistant material should fulfill as many of the following criteria as possible:

1. high flow stress
2. high work hardening rate, resulting in a high strain to plastic instability
3. low stacking fault energy to ensure phase transformation and twinning
4. ductile erosion mechanism
5. no second phase particles or erosion initiating sites in surfaces exposed to cavitation.

CHAPTER 3

REVIEW OF THE PROPERTIES OF WC-Co

WC-Co is a sintered two phase alloy. The microstructure consists of fine angular grains of tungsten carbide cemented together by cobalt. The carbide phase provides hardness, while the ductile binder phase contributes toughness. Variation of the tungsten carbide grain size and the amount of binder gives the appropriate blend of hardness and toughness for a given application.

3.1 CHEMICAL COMPOSITION AND CRYSTALLOGRAPHIC STRUCTURE

3.1.1 Tungsten Carbide

Tungsten forms two hexagonal carbides - the monocarbide WC and the subcarbide W_2C. The crystal structure of tungsten carbide is a simple hexagonal with lattice constants a=2.91Å and c=2.84Å (11,17,25) as shown in Fig. 3.1.

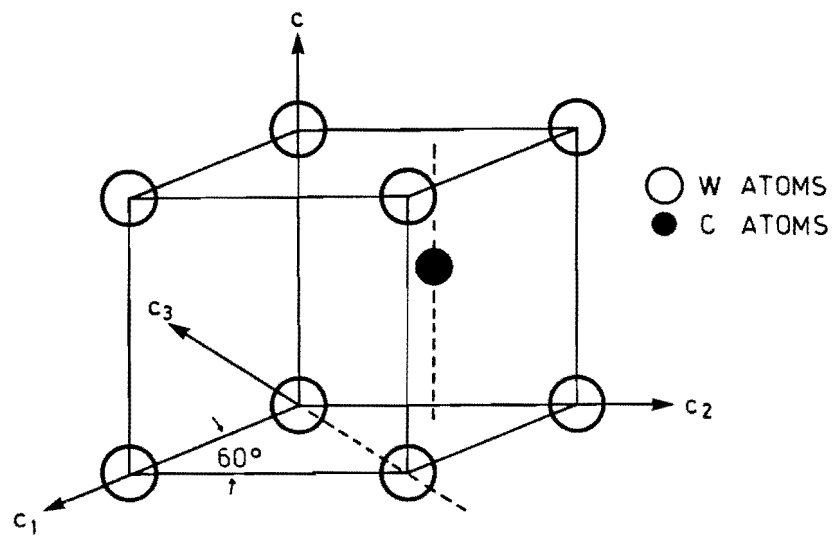

Fig 3.1: Crystal structure of tungsten carbide.

3.1.2 Cobalt Binder

Cobalt is the most common binder metal, due to its good wetting, adhesion in the solid state and adequate mechanical properties. At room temperature the equilibrium structure of cobalt is close-packed hexagonal (hcp). Above 690°K cobalt modifies to a face centred cubic (fcc) structure.

In sintered WC-Co the cobalt is predominantly fcc (1,18,11) due to the restriction in cemented carbides of the transformation (12). The amount of retained fcc is determined by the plastic strain introduced on cooling, the mean free path, the cooling rate and the amount of WC dissolved in the binder (1). The fcc phase is stabilised by dissolved tungsten and carbon in the lattice.

At room temperature the cobalt binder contains 2-10% WC in solid solution (8,11). The tungsten substitutes for cobalt atoms, while the carbon fills the octahedral interstices in the cobalt matrix (8). The hardness of the binder is increased by the WC in solution. Transmission electron microscopy (TEM) studies (5) have shown that the allotropic transformation of the cobalt from fcc $\rightarrow$ hcp could accommodate deformation of sintered carbides at room temperature.

3.1.3 Carbon Content

The range in which the stable two phase WC-Co structure occurs is narrow - the carbon content must be kept within ±0.05 wt% of the stoichiometric composition of 6.12 wt% C. Deficiencies of carbon lead to the formation of eta carbide (W_3Co_3C), while an excess of carbon leads to free graphite.

Both graphite and eta carbide decrease the strength of the alloy (12,30). Eta carbide is precipitated as hard brittle particles and causes local denuding of cobalt leading to structural weakness (30).

3.2 MICROSTRUCTURAL FEATURES

The microstructural features are dictated by the nature of the starting powders and are developed during sintering (1). These features include grain size, mean free path and contiguity and are described below.

3.2.1 Tungsten Carbide Grain Size (d_{WC})

The WC grain size is dependent on the size and distribution of the starting powders, milling and sintering conditions and the composition of the alloy. A few large grains occur due to discontinuous grain growth during oversintering (1).

3.2.2 Mean Free Path (λ)

The mean free path is a measure of the thickness of the cobalt layers and depends on binder content and particle size (12). It can be evaluated by the following expression

$$\lambda = d_{WC} \frac{V_{CO}}{(1 - V_{CO})(1 - C)}$$

where V_{CO} is the volume per cent binder, d_{WC} is the WC grain size and C in the contiguity.

3.2.3 Contiguity (C)

Gurland (22) defines contiguity as the fraction of the total internal surface area of a phase shared by particles of the same phase. There is difficulty in calculating the number of WC-WC grain contacts as there may be a thin layer of cobalt between the grains. Some researchers (6.22.24) assume a continuous carbide "skeleton" in WC-Co alloys containing up to 10-15 vol% cobalt. Exner (11), however, believes that contiguity, while decreasing with increasing binder content, still exists in grades containing over 30 vol% cobalt.

There is no direct evidence of carbide grain contact, but Laugier (21) found that during sintering, some WC aggregates are very stable and could be a source of contiguity in sintered WC-Co alloys.

Each feature can be described by a given parameter and thus be evaluated quantitatively (5). A schematic representation of the microstructural parameters is shown in Fig. 3.2.

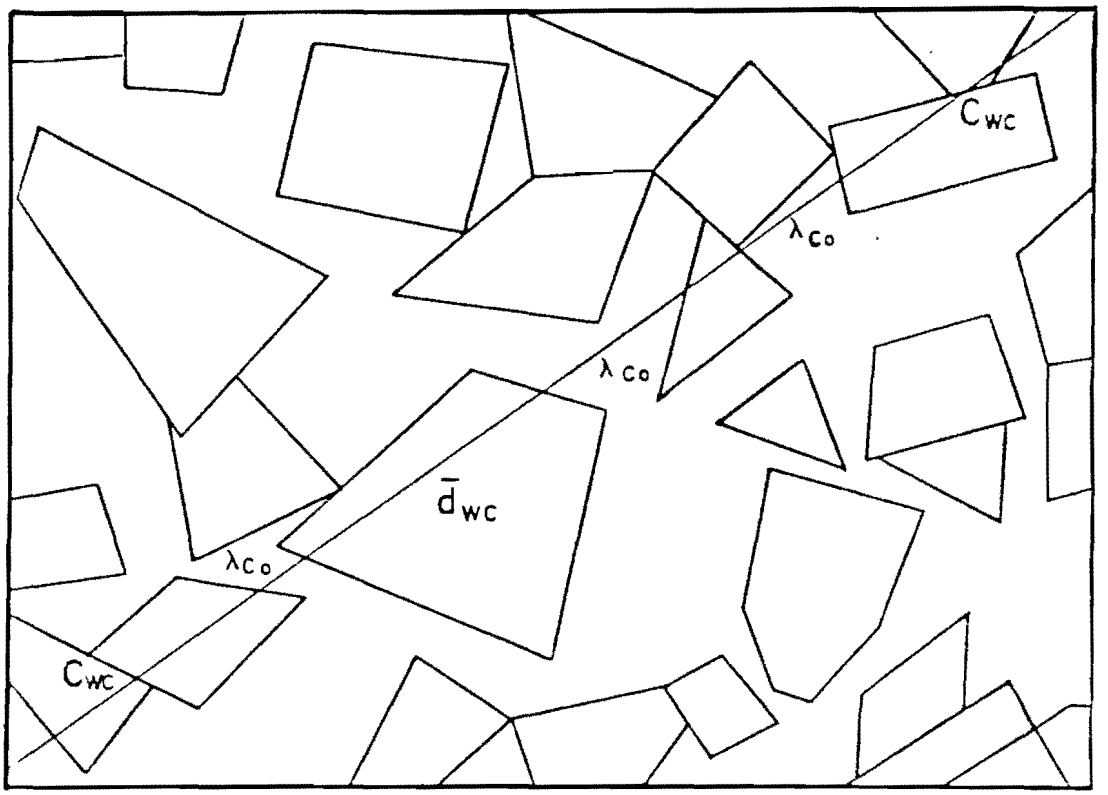

Figure 3.2: Schematic representation of a WC-Co alloy illustrating the microstructural parameters. λ is the mean free path of the binder phase, d_{WC} is the WC grain size and C is the contiguity.

3.3 PHYSICAL PROPERTIES

3.3.1 Youngs Modulus

The Youngs modulus of WC-Co decreases with increasing binder content. For a small size distribution, grain size has minimal influence on the Youngs modulus (6,26).

Simple theories such as the law of mixtures can account grossly for the dependence of Youngs modulus on binder content. For the law of mixtures the lower bound (minimum modulus) represents the elastic behaviour of laminated materials with the plane of the laminates normal to the direction of applied force (fig. 3.3a). The distribution of stress under load is then uniform throughout the specimen. The upper bound represents the elastic behaviour of oriented filament reinforced composites (fig. 3b), where the distribution of strain under load is uniform.

A more stringent set of bounds proposed by Hashin and Shtrikman (in Doi et al (9)) corresponds to two inclusion models. The upper bound corresponds to soft spherical inclusions (Co) in a hard matrix (WC), while the lower bound represents hard spherical inclusions in a soft matrix. For WC-Co alloys these models are successively valid - the upper bound model for alloys with less than 16 vol-% cobalt and the lower bound model for alloys with more than 16 vol-% cobalt (6).

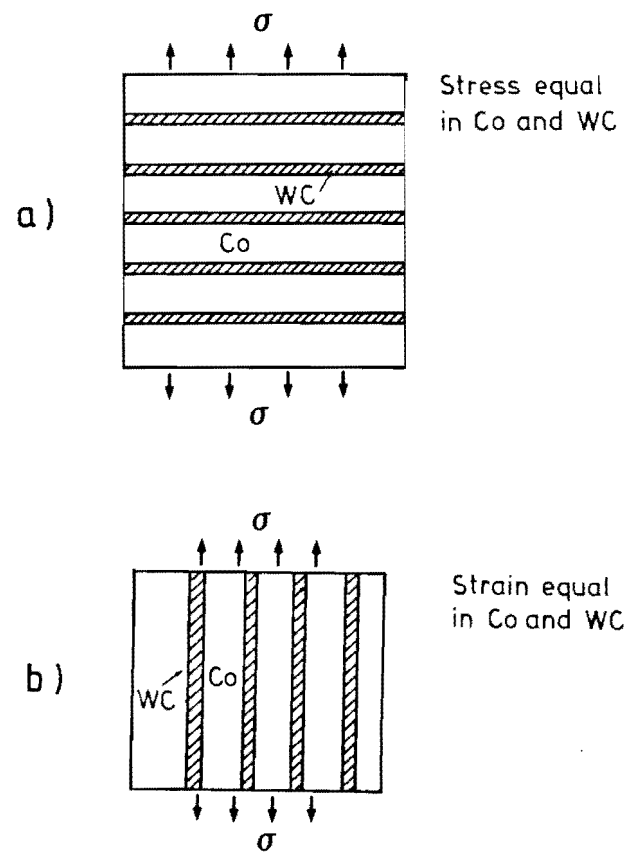

Figure 3.3: A fibre-reinforced composite loaded so as to give (a) minimum modulus and (b) maximum modulus.

Values for the Youngs modulus of WC from these models were in agreement with the published results while the Youngs modulus of the cobalt binder was found to be higher than that for pure cobalt. This was attributed to the stress state of the binder and the dissolution of the WC in the cobalt. These models are shown in section 6.2.3 with experimental results.

3.3.2 Residual Stresses

3.3.2.1 Thermal Stresses

On cooling the WC-Co alloy from the sintering temperature, thermal stresses are introduced. The thermal expansion coefficient of cobalt is approximately three times that of tungsten carbide. This results in compressive stresses being set up in the WC and triaxial tensile stresses in the binder on cooling (11,12)

3.3.2.2 Mechanically Introduced Stresses

The thermally induced stress patterns can be modified by mechanical treatment (11). Grinding has a pronounced influence on the residual stress pattern in WC-Co alloys. Compressive stresses are introduced near the surface, which reduce or convert the tensile stress in the cobalt to a compressive stress, while increasing the stress level in the carbide phase.

3.4 MECHANICAL PROPERTIES

Toughness and hardness of WC-Co are both strongly dependent on the microstructural properties.

3.4.1 Hardness

Hardness decreases with increasing binder content and increasing grain size as shown in Fig. 3.4a. An apparently simple function between hardness and mean free path (Fig 3.4b) has been observed (12 & 28), but on closer analysis it was found that additional parameters such as particle size and composition are necessary to describe the relationship precisely. Eta carbide has been associated with a small increase in hardness (30).

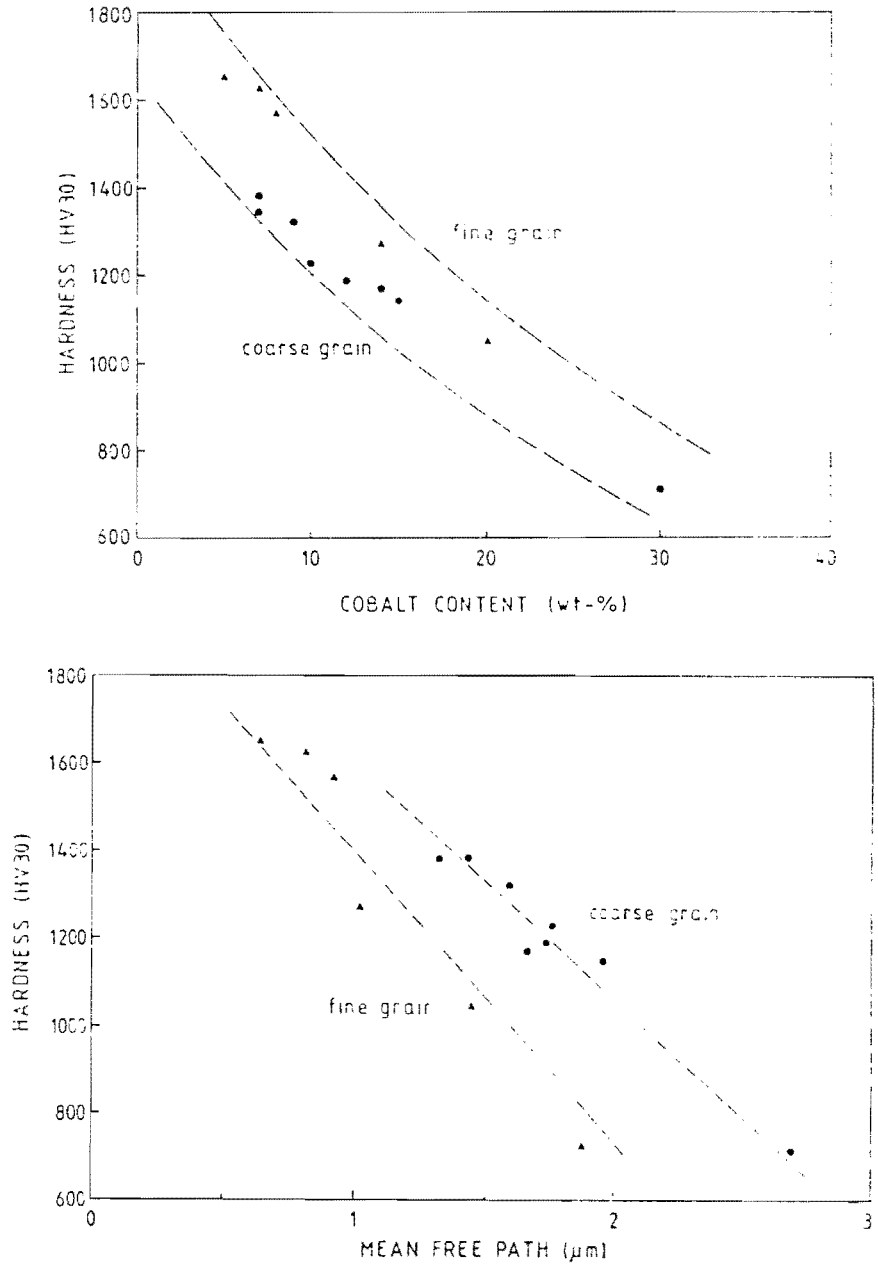

Figure 3.4: The effect of (a) cobalt content and (b) mean free path on hardness of WC-Co (after Pennefather (28)).

3.4.2 Transverse Rupture Strength

Transverse rupture strength (TRS) is a measure of the resistance of WC-Co to fracture. TRS increases with mean free path to a maximum, then decreases (Fig 3.5). The maximum is dependent on the cobalt content (12,15).

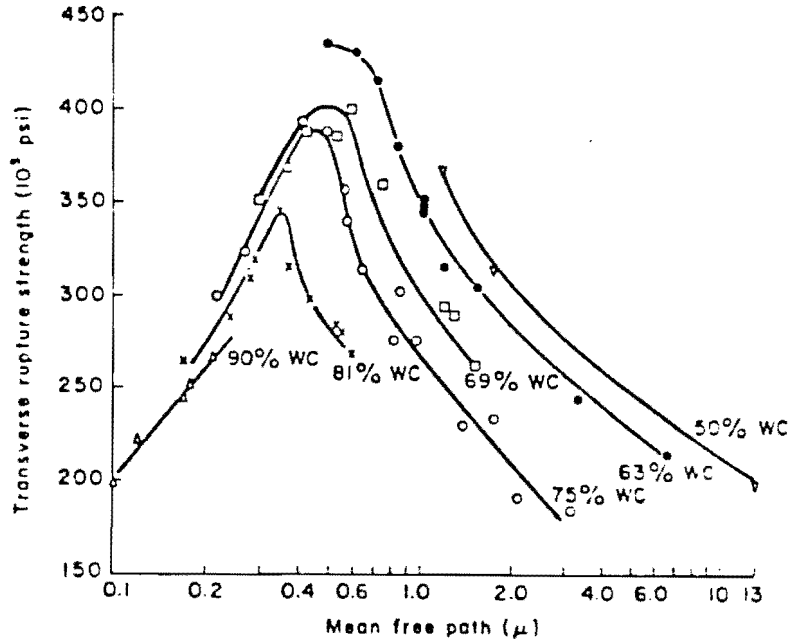

Figure 3.5: Transverse rupture strength as a function of mean free path (after Gurland and Parikh (15)).

The maximum has been explained by a change in fracture mode (17,15,30). A gradual change in the structure from a WC "skeleton" to WC "embedded" in cobalt occurs as the mean free patn increases. The initial increase in TRS with increasing mean free path and binder content is due to a decrease in plastic constraint of the binder. Plastic flow is thus easier and local stress concentrations are relieved. This impedes crack initiation and propagation.

The ensuing decrease of TRS with increasing mean free path can be explained by dispersion hardening: the flow strength of the binder is reduced as the carbide particle spacing becomes greater.

TRS decreases with decarburisation, which results in the formation of eta carbide (W_3Co_3C). The brittle eta phase acts as a stress raiser and removes cobalt from the binder.

3.4.3 Fracture Toughness

As WC-Co alloys generally fail by brittle fracture at normal temperatures, toughness is a measure of their resistance to fracture. This results in a blurring of the distinction between strength and toughness. There is a difference in the dependance of strength and toughness on the mean free path, however: fracture toughness increases smoothly with increased mean free path (see Figure 3.6), whereas strength increases to a maximum as explained in section 3.4.2.

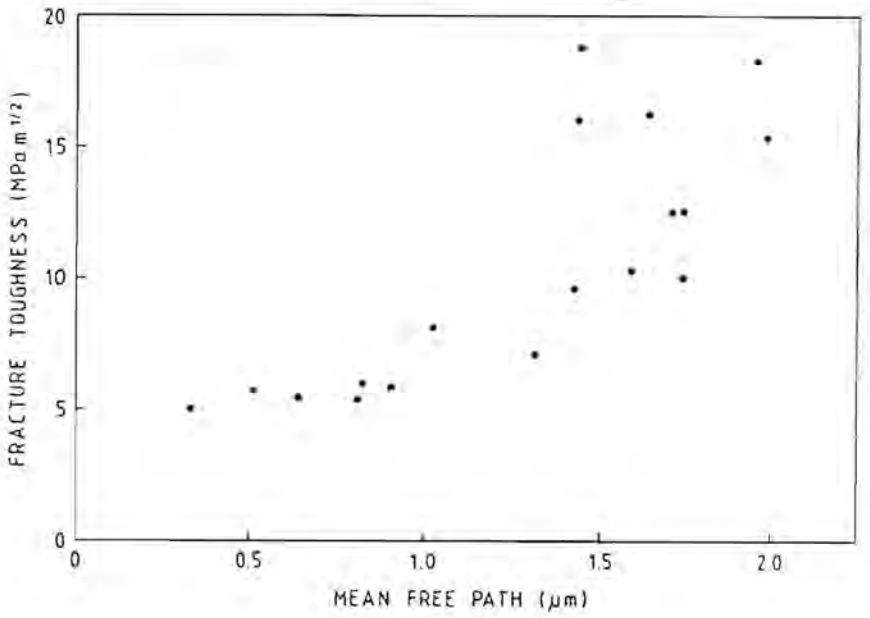

Figure 3.6: Fracture toughness as a function of binder mean free path for WC-Co alloys (after Pennefather (28)).

There are a large number of experimental methods available for determining the fracture toughness of cemented carbides, but as yet there is not a standard test. These tests include the three point bending test used by Chermant et al (6); the double torsion test used by Murray (26) and the Palmqvist indentation test used by

Peters and Cooper (30), Shetty et al (36) and Pennefather (28). As the fracture toughness of the WC-Co alloys used in this study were determined using the Palmqvist technique, only this test will be described here.

3.4.3.1 Palmqvist Test

Palmqvist developed the idea of testing the toughness of cemented carbides using cracks formed at the corners of a Vickers hardness indentation (36). It was found (27,35) that in WC-Co alloys containing greater than 5 wt% cobalt, Palmqvist cracks (Fig. 3.7b) were formed and not half-penny cracks (Fig 3.7a).

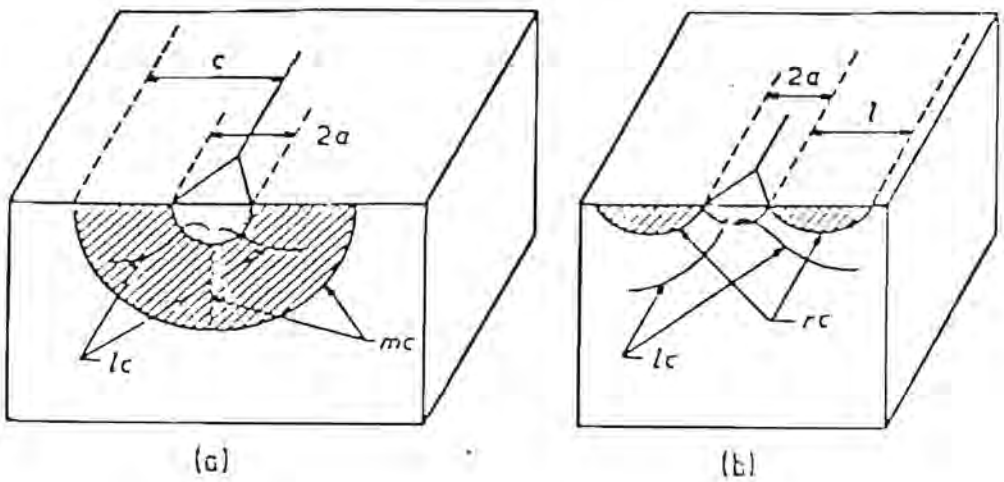

Figure 3.7: Indentation showing (a) half-penny cracking and (b) Palmqvist cracking, where 'a' is half the diagonal length, 'c' is the crack length for a half-penny crack and 'l' is the Palmqvist crack length (after Niihara et al (27)).

The Palmqvist toughness is defined as

$$W = P/L \qquad (3.2)$$

where P is the load and L is the sum of the four crack lengths measured at the indentation corners (29).

Exner et al (13) and Peters (29) found an empirical linear relationship betwen W and the energy release rate (G_{IC}) which is valid for low binder alloys. Murray (26) showed that G_{IC} should vary linearly with mean free path, thus the Palmqvist toughness should (and does) increase with increasing mean free path.

Considerable interest has been shown in developing a relationship between the fracture toughness (K_{IC}) and W. Evans and Charles (10) showed that the relationship between fracture toughness and the ratio of crack-to-indent size exhibited universal behaviour. For half-penny cracks in a variety of materials this relationship can be described by equation 3.3.

$$\left(\frac{K_{IC}\phi}{H\ a^{\frac{1}{2}}}\right)\left(\frac{H}{E\phi}\right)^{0.4} = 0.129\ (c/a)^{-1\ 5} \qquad (3.3)$$

where H is the hardness, E the Youngs modulus, ϕ is a constant factor and c,a and l are defined in Figure 3.6.

Niihara et al (27) modified this analysis to account for the change in crack geometry associated with Palmqvist cracks (equation 3.4).

$$\left(\frac{K_{IC}\phi}{H\ a^{\frac{1}{2}}}\right)\left(\frac{H}{E\phi}\right)^{0.4} = 0.035\ (l/a)^{-0\ 5} \qquad (3.3)$$

Laugier (21) found equation 3.2 to give a better estimation of fracture toughness for WC-Co alloys, while Shetty and Wright (35) considered equation 3.3 to give the better estimation. Shetty and Wright argued that the selection of a particular approach to analysis of indentation data should not be based purely on correlation of estimated and measured values of K_{IC}, as the two available models are only approximations of the actual problem. Instead a correct fracture mechanic interpretation of Palmqvist cracks is required.

The Palmqvist method is not universally accepted as a measure of fracture toughness, mainly as its basis is empirical and not theoretical. The method is, however, a simple, inexpensive and non-destructive technique for evaluating and comparing commercial WC-Co alloys (13,29). Principal drawbacks to the method are sensitivity to surface finish and restriction to materials containing less than 15 wt% cobalt.

CHAPTER 4

A REVIEW OF THE EROSION OF WC-Co

WC-Co cermets are considered to undergo a mixed mode of erosion due to the two phase nature of these alloys. Pennefather (28) and Wright et al (42) observed brittle fracture of the tungsten carbide grains and ductile deformation of the cobalt binder. Microstructural properties are thus an important consideration when studying the erosion of WC-Co alloys.

4.1 VARIABLES AFFECTING THE EROSION OF WC-Co ALLOYS

Hardness and fracture toughness are considered to be important properties affecting erosion. Both are dependent on the binder content and thus it is of interest to study erosion rate as a function of cobalt content.

Conrad et al (7) found that for solid particle impact erosion, erosion rate (measured as the slope of the steady state portion of the erosion curve) generally increases with increasing binder content. A similar result was found by Shetty et al (36) for slurry erosion tests. However, Ball and Paterson (3) and Pennefather (28) found that for solid particle impact erosion at high impact angles (the angle of impact is the inclination between the target surface and the particle trajectory), erosion rate did not increase monotonically with binder content. A maximum in erosion rate was observed at 10 wt-% cobalt and a minimum was found at 20 wt-% cobalt. The models proposed by these authors are explained in detail in Section 4.3.2.

Heathcock (16) found that for cavitation erosion of cemented carbides, the two nickel based cermets tested showed decreased erosion resistance with increasing binder content. Cobalt based cermets, however, did not follow this trend. A minimum in erosion rate was found at 15 wt-% cobalt. The model proposed for this behaviour is explained in detail in Section 4.3.1.

Tungsten carbide grain size is known to affect the erosion rate of WC-Co alloys. Heathcock (16) found that an increase in grain size resulted in increased cavitation erosion for the cobalt based alloys tested. Conrad et al (7) observed a maximum in particle erosion rate at a grain size of 1.5 μm. Pennefather (28), for tests at high angles, found a higher

particle erosion rate for smaller grain sized alloys. The actual effect of grain size is neither fully understood nor agreed upon.

The exceptional cavitation erosion resistance observed for cobalt based alloys such as Stellites (14), was thought to be due to the strain induced martensitic type transformation of the cobalt. Woodford (4), however found no correlation between erosion resistance and any simple measure of transformation for Haynes Stellite 6B. He attributed the good erosion resistance to the planar slip mode, which is a result of the low stacking fault energy (SFE) of the cobalt, and delays fatigue crack nucleation. As a decrease in SFE increases the possibility of transformation, any transformation of the cobalt may thus be considered incidental rather than instrumental in controlling erosion resistance. Antony and Silence (2) proposed that energy absorbed by the transformation explains the variation in incubation period shown by cobalt alloys, but does not adequately explain the low steady state erosion rates. They suggest that the benefit derived from the fcc→hcp transfomation is due to the high strain energy to fracture of the hcp phase rather than from the energy absorption during transformation.

Heathcock (16) suggested that the state of internal stress is an important factor in controlling the cavitation erosion resistance of cemented carbides. The residual stresses generated on cooling from the sintering temperature (due to the difference in thermal contraction coefficients of the carbide phase and the binder) result in the carbide grains being subjected to a triaxial compressive stress and the binder to a triaxial tensile stress. Heathcock calculated the residual stresses of the WC-Co alloys used to be of the order of 1200 MPa. In the cobalt based cermets the residual stress pattern is also affected by the volumetric contraction associated with the allotropic fcc→hcp transformation (see Section 4.3.1).

4.2 MODES OF MATERIAL REMOVAL

Various modes of material removal have been reported for particle erosion (3,7), abrasion (20) and cavitation erosion (16) of cemented carbides, but in all the proposed mechanisms, cobalt removal is apparently the initial and rate controlling step. Heathcock (16) suggests that,for cavitation erosion, the binder is preferentially eroded, followed by the removal of WC grains when there is no longer sufficient binder to hold

them. The removal of cobalt is initiated at binder-carbide interfaces and a considerable amount of cobalt is removed prior to WC pull-out.

4.3 MODELS OF EROSION

4.3.1 Cavitation Erosion

Heathcock (16) studied a range of cemented carbides, two with nickel binder and eight with cobalt binder. Figure 4.1 shows the effect of binder type, binder content and carbide grain size on the erosion resistance of the various cemented carbides.

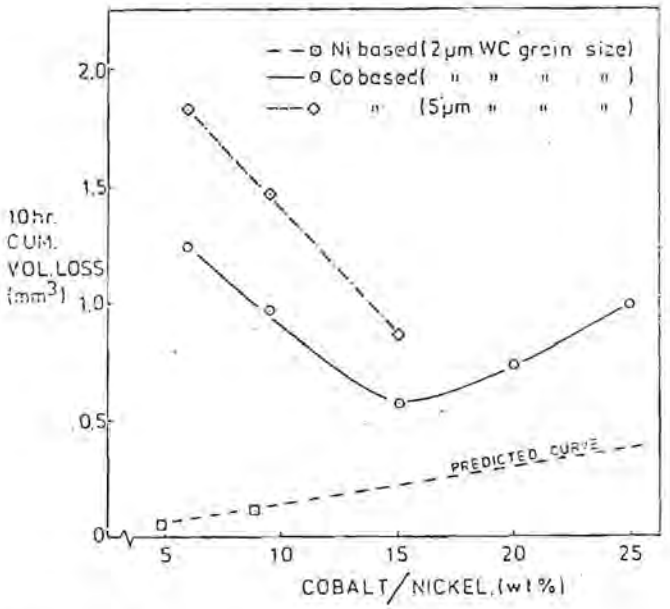

Figure 4.1: The effect of binder type, binder content and carbide particle size on the erosion of cemented carbides (after Heathcock (16)).

The nickel based cermets were found to be more erosion resistant than those with cobalt binder, despite the better adhesion of cobalt to tungsten carbide in the solid state. Heathcock suggested that this was due to the stress state of the binder.

As previously mentioned (Section 4.1), both binder metals suffer residual stresses as a result of the variation in thermal contraction coefficients between the carbide and the binder. Cobalt, however, shows a volumetric contraction associated with the allotropic fcc → hcp phase transformation. This results in an increase in the tensile stresses in the cobalt, leading to a

weakening of the cobalt-carbide bond. In some cases this could lead to debonding.

As cobalt removal is initiated at cobalt-carbide interfaces, this debonding would give rise to an increase in the erosion rate of the cermet. Heathcock followed the phase change by X-ray diffraction and found that the cobalt based samples were all partially transformed as a result of mechanical prepolishing but that further transformation occurred during the erosion test. Heathcock found that the nickel based grades did not undergo a phase transformation during cavitation erosion and suggested that this could explain their higher erosion resistance.

For the cobalt based alloys, a minimum in cavitation erosion (maximum erosion resistance) was found at 15 wt-%. Below this value, a decrease in the binder content is associated with a rapid increase in contiguity of the carbide grains. This leads to an increase in the rigidity of the WC skeleton and a greater ability to withstand transition induced stresses. This, however, promotes cracking at the carbide-cobalt interface, offsetting any hardening of the binder due to increased plastic constraint. The cobalt is thus more easily removed and the erosion rate increases.

Above 15 wt-% the cobalt based alloys show the expected monotonic decrease in erosion resistance with increasing binder content. This is considered to be a result of decreased plastic constraint, and therefore decreased hardness of the binder, associated with an increase in the mean free path of the binder. The decrease in erosion resistance of the binder lowers the resistance of the composite.

The increase in erosion with increased grain size is attributed to an increase in binder mean free path. The accompanying decrease in plastic constraint of the binder results in a decreased hardness and hence increased erosion of the cobalt.

4.3.2 Particle Erosion

Ball and Paterson (3) carried out solid particle impact erosion tests on a range of WC-Co alloys, with particle velocity and angle of impact parameters of $40ms^{-1}$ and 45° respectively. As mentioned previously (Section 4.1) the erosion rate did not increase with increasing binder content. The relationship found is illustrated in fig. 4.2. No quantitative relationship was formulated, but a qualitative model of erosion was postulated.

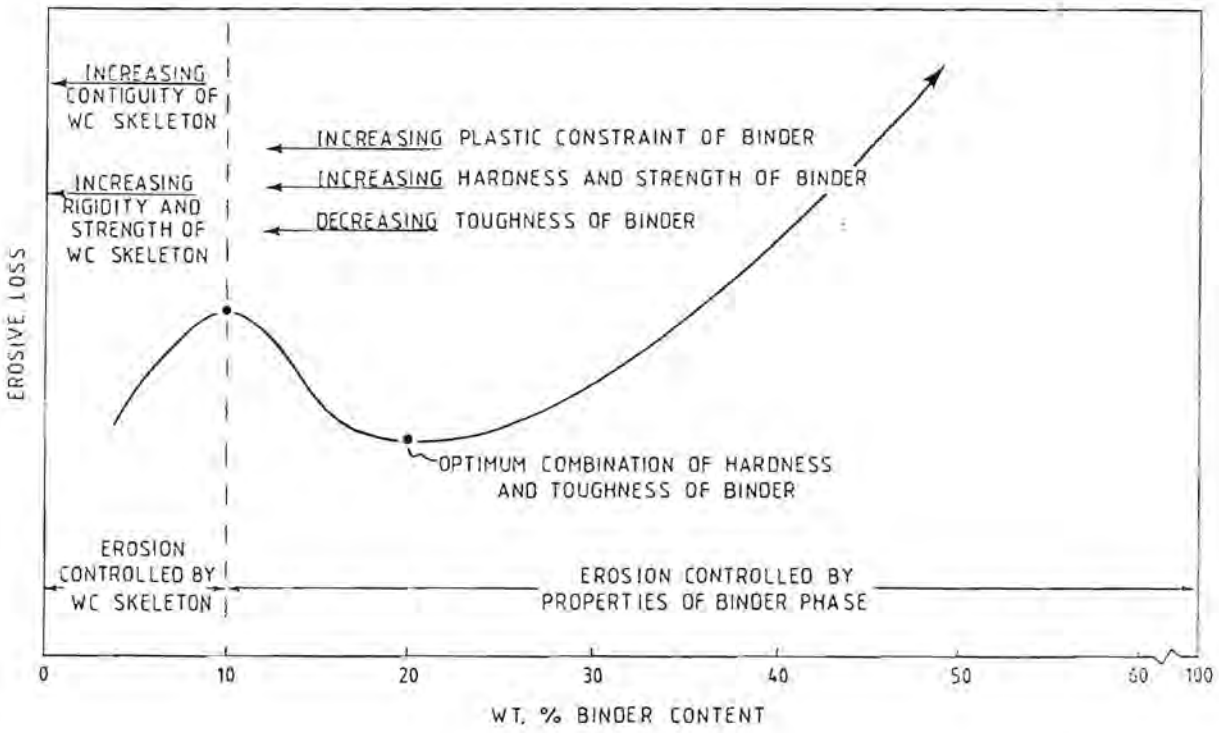

Figure 4.2: A schematic representation of the erosion of WC-Co alloys as a function of binder content. The factors which are considered to control erosion are indicated (after Ball and Paterson (3)).

The local maximum at 10 wt-% cobalt was explained in terms of a change in microstructure. Below 10 wt-% the erosion is controlled by the WC skeleton. As the contiguity increases, the skeleton becomes more rigid and the erosion rate decreases. A more rigid skeleton is, however, usually associated with brittle erosion, causing an increase in erosion to be expected. This indicated that an underlying mechanism, which is not immediately apparent, must be

responsible for the decrease in erosion. Above 10 wt-%, erosion is controlled by the strength and microstructure of the binder. At 10 wt-% the WC skeleton is fragile and discontinuous, and the cobalt has low toughness.

The minimum in erosion at 20 wt-% cobalt was explained as the result of an optimum combination of hardness and toughness of the binder. No mechanism for the change in erosion rate was proposed by the model.

Pennefather (28) confirmed and extended Ball and Paterson's model in a study of solid particle erosion of nineteen grades of WC-Co alloys. The influence of various parameters such as particle velocity and angle of impact was investigated. At low impact angles, an increase in erosion rate with increasing binder content occurred, but at higher angles, a maximum in erosion rate was found at approximately 10 wt-% cobalt. The Pennefather model for particle erosion of WC-Co alloys for angles of incidence greater than or equal to 45° is shown in fig. 4.3.

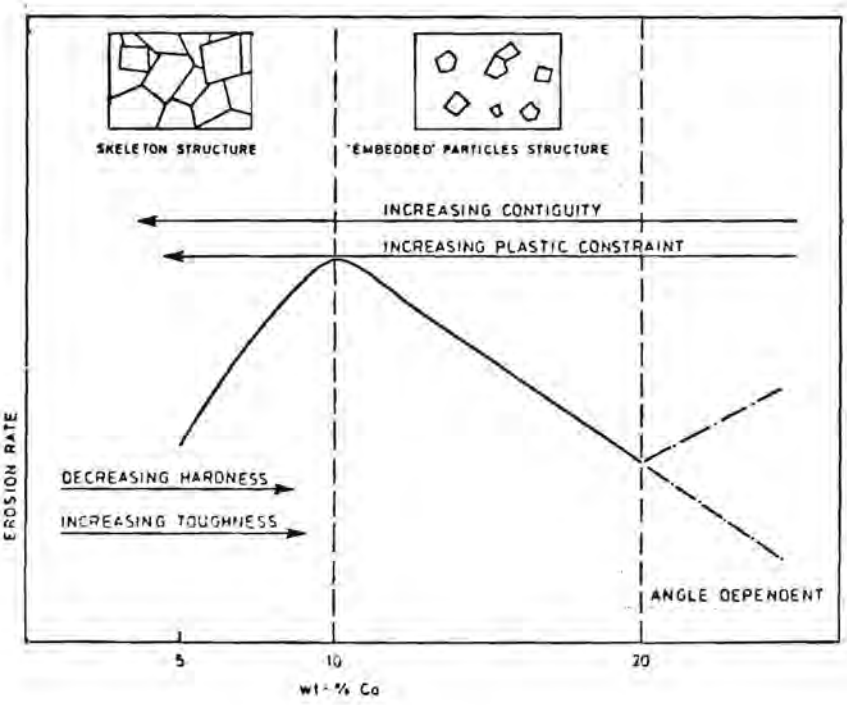

Figure 4.3: A schematic summary of erosion processes in WC-Co alloys. The parameters believed to affect erosion rate are indicated (after Pennefather (28)).

The model can be divided into three regions according to the mechanism of material removal. Below 10 wt-% cobalt, the load is transferred through the rigid WC skeleton; cobalt extrusion is predominant and little WC grain fracture occurs. As the binder content increases and the skeleton weakens, more carbide fracture occurs. Between 10 and 20 wt-% binder there is a structure change towards more embedded grains. The decrease in contiguity means that less grains touch, resulting in a reduction in WC grain fracture, which leads to a decrease in erosion rate. Above 20 wt-% cobalt the WC grains are mainly embedded and erosion occurs mainly by a ductile mechanism. Limited carbide grain fracture, however, still occurs. The three modes of material removal, cobalt extrusion, WC cracking and ductile cutting, all occur at any binder level; however, the predominant mode depends on the binder content.

The erosion of the WC-Co alloys is considered to be a combination of ductile and brittle modes of material removal. The importance of each mode was found to be dependent on both angle of impact and particle size. At high angles of impact and with large erodent particle size the brittle mode was found to predominate.

CHAPTER 5

EXPERIMENTAL TECHNIQUES

A range of previously characterised (see Chapter 6), commercially available WC-Co alloys were subjected to cavitation erosion and further characterised, using the following techniques.

5.1 VIBRATORY CAVITATION

The most common way of assessing cavitation damage is weight or volume loss as a function of exposure time. These curves can be divided into two main regions:

1. Incubation period - this has been described in a number of ways (2,43). In this study it is measured as the X-intercept of an extrapolation of the steady state volume loss rate. During this period deformation of the surface occurs with little or no material loss.
2. Steady state - here the erosion rate, having reached its maximum, is constant.

The parameters on which erosion resistance may be based are incubation period (t_0), cumulative volume loss (CVL) and rate of volume loss in steady state region ($\dot{\epsilon}$). These are determined as illustrated in fig. 5.1. It is necessary to consider more than one parameter to obtain a true assessment of material performance, since an evaluation based on a single parameter can be misleading. Mechanical and microstructural parameters such as hardness and contiguity must also be considered.

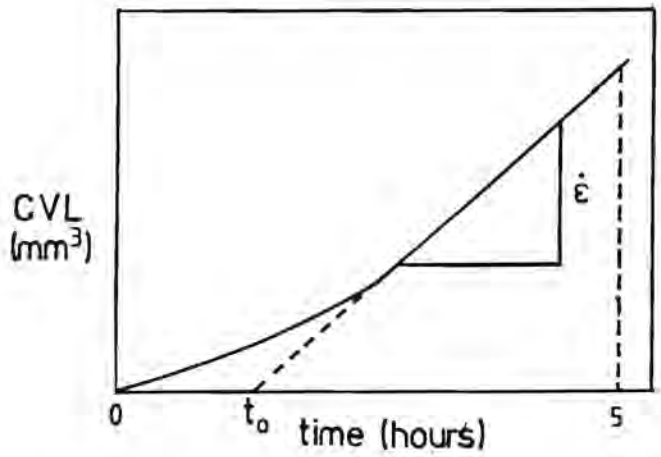

Figure 5.1: Determination of incubation time, erosion rate and five hour volume loss from cumulative volume loss-time graph.

5.1.1 VIbratory Cavitation Equipment

The vibratory cavitation equipment used was that constructed by Heathcock (16). A stationary specimen mount, such as used by Vyas and Preece (38) was used rather than the vibratory specimen as recommended by the ASTM standard method G32-72. This was to avoid longitudinal stresses, which can cause fatigue failure of the specimen.

The apparatus is shown in fig. 5.2 and consists of a piezoelectric transducer which vibrates at a frequency of approximately 20kHz. An exponential velocity transformer or "horn" amplifies the oscillations produced by the piezoelectric transducer by a factor of approximately 3.5. The amplitude is determined optically by measuring the vertical expansion of a horizontal machining mark in the drill tip when the drill is operating. The size of this extended point is measured against a calibrated graticule and adjusted to give the correct amplitude, with a precision of approximately 3 μm.

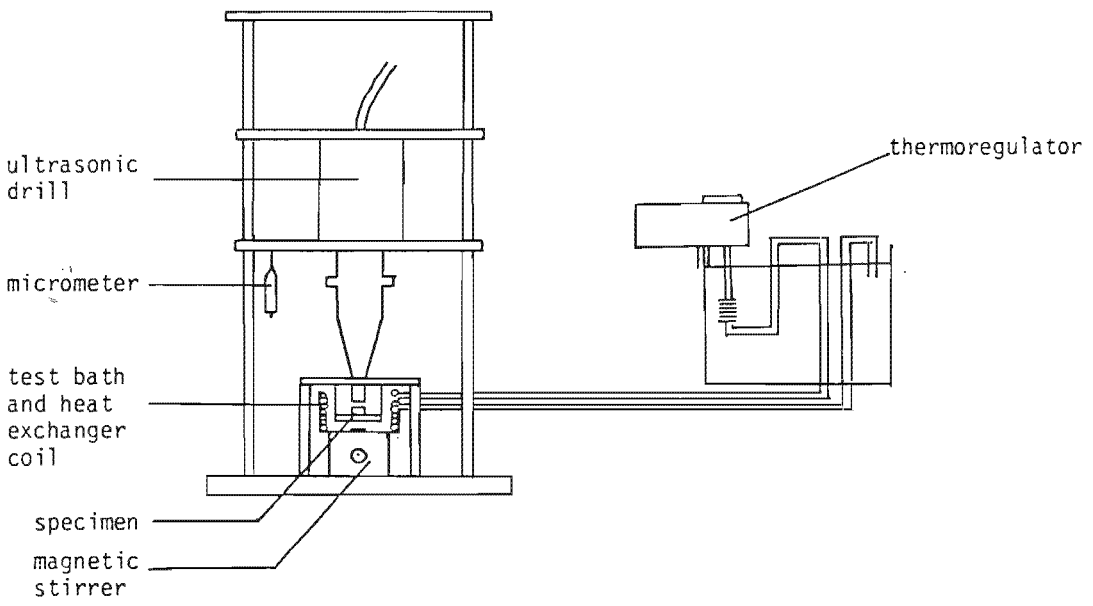

Figure 5.2: Vibratory cavitation erosion test apparatus

The pressure change in the liquid in the cavitation zone is inversely related to the separation distance, and determines the intensity of cavitation. Maximum erosion occurs at a critical separation distance d_{crit}. Below this value the temperature of the

fluid in the gap increases, which increases the vapour content of the cavities. This leads to a cushioning effect and a decrease in erosion (37). Heathcock (16) determined the erosion of pure iron in distilled water as a function of distance between the drill tip and the specimen on the same rig. As shown in fig. 5.3, a maximum was found at 0.35mm, and thus this separation distance was used in both his and the present studies.

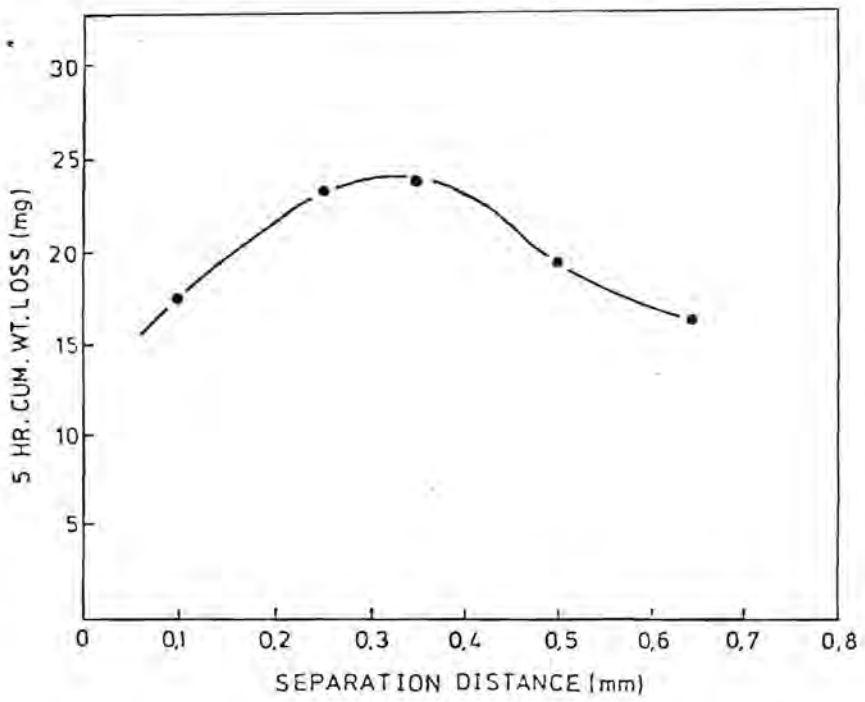

Figure 5.3: Erosion of pure iron as a function of separation distance (after Heathcock (16))

5.2 SPECIMEN PREPARATION

The WC-Co samples used were 14mm diameter discs. They were polished prior to testing using the method determined by Pennefather (28), to obtain a constant stress level corresponding to the equilibrium thermal stresses. This method is outlined below:

(i) x hours on an automatic polisher with 15 μm diamond paste
(ii) 15 minutes polishing with 6 μm diamond paste
(iii) 15 minutes polishing with 3 μm diamond paste
(iv) 5 minutes polishing with 1 μm diamond paste

The polishing time on the automatic polisher with 15 μm diamond paste varies according to cobalt content. Low binder content grades are harder and thus need longer polishing times to remove the stresses introduced by grinding and erosion. The alloys were tested in the as received condition

5.3 TYPICAL TEST PROCEDURE

1. The distilled water in the test bath and the drill tip at the end of the drill horn are replaced before each new sample is tested.
2. The vibratory equipment is warmed up for one hour prior to testing to allow the horn to reach equilibrium temperature. The temperature in the test bath is maintained at 25°C by the circulation of regulated water through a heat exchange coil.
3. A polished specimen which has been notched (for orientation) and weighed is inserted into an insulated sample holder. A polished and weighed sample is placed in the test bath as a dummy sample to monitor the corrosion effect.
4. A separation distance of 0.35mm between specimen and drill tip is set using the micrometer.
5. Both samples are removed after one hour, ultrasonically cleaned in alcohol, dried and weighed to 0.1mg accuracy.
6. X-ray diffraction (XRD) is done on the eroded sample and both samples are examined in the SEM. Both samples are then replaced in the rig. Each sample is tested for 5 hours, by which time the cavitation eroded sample has reached steady state.

5.4 SCANNING ELECTRON MICROSCOPY

Each sample was examined under the SEM during the course of the test to determine a mode of material removal. The samples were gold-palladium coated for the final (5 hour) examination, but not during the course of the test.

5.5 X RAY DIFFRACTION (XRD)

The allotropic phase change of the binder (fcc $\longrightarrow$ hcp) occuring during the test was followed by XRD. Cu K_α radiation was used with a monochromator to eliminate reflections from the K_β radiation. X-ray diffraction traces were done for both polished and eroded samples. For a small range of alloys, traces were taken during the course of the cavitation erosion test. The

ratio of the intensities of the $(101)_{hcp}$ and $(111)_{fcc}$ peaks was used as an indication of the transformation of binder during cavitation erosion. The percentage increase in transformation after 5 hours of cavitation was calculated from the initial (polished) and final (eroded) hcp/fcc ratios.

$$\% \text{ increase in transformation} = \left(\frac{(hcp/fcc)_{final}}{(hcp/fcc)_{initial}} \right) - 1 \quad \times 100 \qquad (5.1)$$

5.6 DENSITY TESTS

Density measurements were obtained using the Standard Test Method for Density of Cemented Carbides (ASTM B311-58). The volume per cent binder for each sample was calculated from the density.

5.7 YOUNGS MODULUS MEASUREMENTS

The Youngs modulus values were determined using the in-plane resonance of the thin discs. Disk resonances fall into two series. In the first, the distortion modes are nodal diameters which divide the disc into slices, adjacent slices vibrating in and out in reverse phases. The actual area is unchanged (fig. 5.4a). In the second series, the whole periphery expands and contracts, resulting in an area change (fig. 5.4b)

A comparison of two modes, one from each series, gives Poisson's ratio with good sensitivity. For these measurements, the (1,R) and (1,3) modes were used as they are at adjacent frequencies without being close enough to interact. The calculation of the Youngs modulus of the WC-Co alloys from these parameters is given in Appendix 1.

The transmission line technique used was that developed for material characterisation up to very high temperatures by Bell and Sharp (4). One end of a long nickel wire of diameter 0.7mm was flattened and cemented to the top surface of the disk. A burst of oscillations from the magnetostrictive transducer at the remote end of the line drives the resonator (specimen) and the return signals are detected by the same transducer (fig. 5.5).

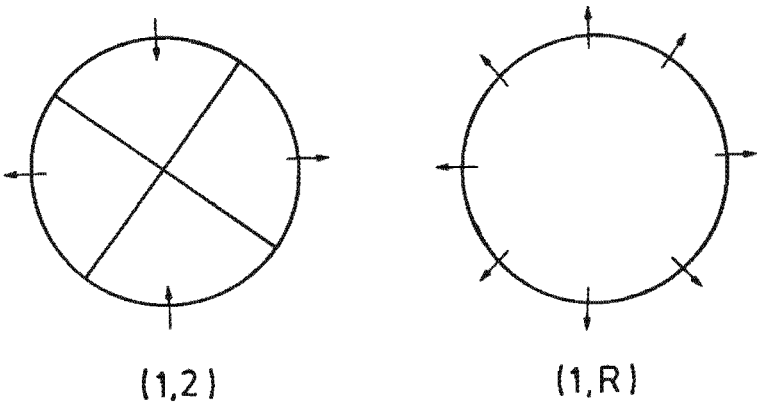

Figure 5.4 a & b: Fundamental modes of the two distortion resonance series

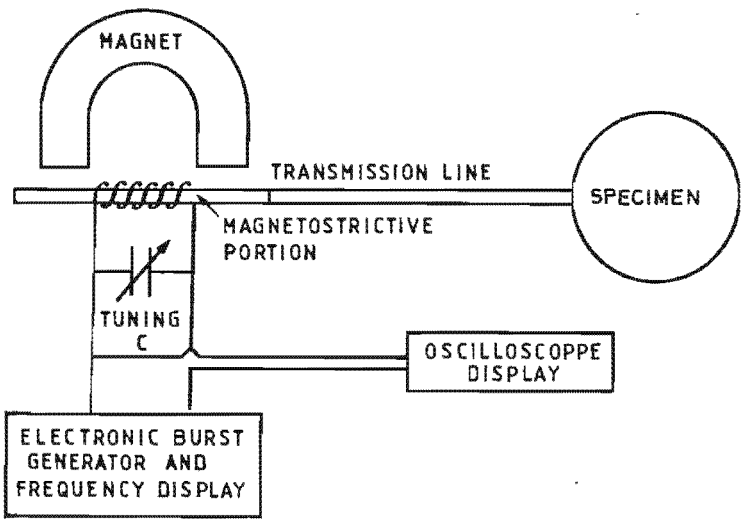

Figure 5.5: The basic transmission line system used for determining the Youngs modulus of the WC-Co alloys (after Bell and Sharp (4)).

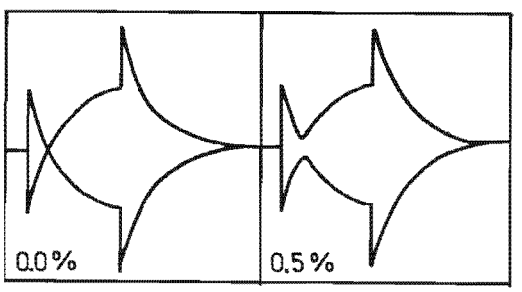

Figure 5.6: Echo characteristics showing the crossover null which identifies resonance.

The signal returned from the specimen is displayed on an oscilloscope. The crossover null which identifies resonance is shown in fig. 5.6. The resonance frequencies of the two modes of interest, the (1,3) and the (1,R), are then taken from the frequency display.

A computer program, shown in Appendix 1, was written to calculate the Youngs modulus from the two measured resonances, the density and the diameter for each sample.

5.8 HARDNESS

The hardness of the WC-Co alloys were tested using the Vickers diamond pyramid indentor, using a load of 30kg. An average of four values was taken.

CHAPTER 6

RESULTS

The WC-Co alloys used in this study are commercially available grades. The same set of alloys was used previously by Pennefather (28) during a study on solid particle erosion of WC-Co. These results are included in this section, along with other microstructural parameters and mechanical properties obtained during the present study. The results of scanning electron microscopy will also be presented.

6.1 MICROSTRUCTURAL PARAMETERS OF THE WC-Co ALLOYS INVESTIGATED

The grain size, binder mean free path and contiguity values used in this study are those obtained by Pennefather (28) for the same set of samples and are listed in Table 6.1. These values were determined using lineal analysis.

Table 6.1 The nominal grain size, mean free path and contiguity of the WC-Co alloys (from Pennefather (28)).

GRADE	NOMINAL GRAIN SIZE (μm)	MEAN FREE PATH (μm)	CONTIGUITY
A1	1.46	0.642	0.790
B1	1.85	0.810	0.773
B2	1.88	0.927	0.670
B3	1.78	1.024	0.570
B4	1.76	1.436	0.475
F1	2.98	1.317	0.715
F2	2.83	1.729	0.604
F3	2.85	1.950	0.540
G1	2.80	1.425	0.710
G2	2.64	1.581	0.694
G3	2.82	1.740	0.673
G4	2.58	1.637	0.556
I1	2.17	2.690	0.392
C1	2.42	0.823	0.728
C2	2.00	1.435	0.630
H1	3.31	1.714	0.680
H2	3.00	1.986	0.550
D1	1.28	0.510	0.660
E1	0.56	0.330	0.831

The lineal analysis results suggested that the majority of the grades could be divided into two groups based on grain size. The first group consisted of the A and B grades, with an approximate nominal grain size of 1.8 μm, while the F, G and I grades had an approximate nominal grain size of 2.8 μm. In situations where the effect of grain size is studied, only those grades falling into these two grain size groups were used.

Mean free path is dependent on binder content and grain size, as shown in fig. 6.1. This is expected from the equation defining mean free path (see Section 3.2.2).

Contiguity, the degree of contact between carbide particles, decreases with increasing cobalt content, as shown in fig. 6.2. As noted by Lee and Gurland (22), contiguity increases with increasing grain size.

The volume per cent binder was calculated from the measured densities of the alloys. These values are compared with those determined by Boart and those obtained by Pennefather (28) using lineal analysis for the same set of samples (see Table 6.2). The correlation between the supplier's values, Pennefather's results and the experimental values was considered acceptable.

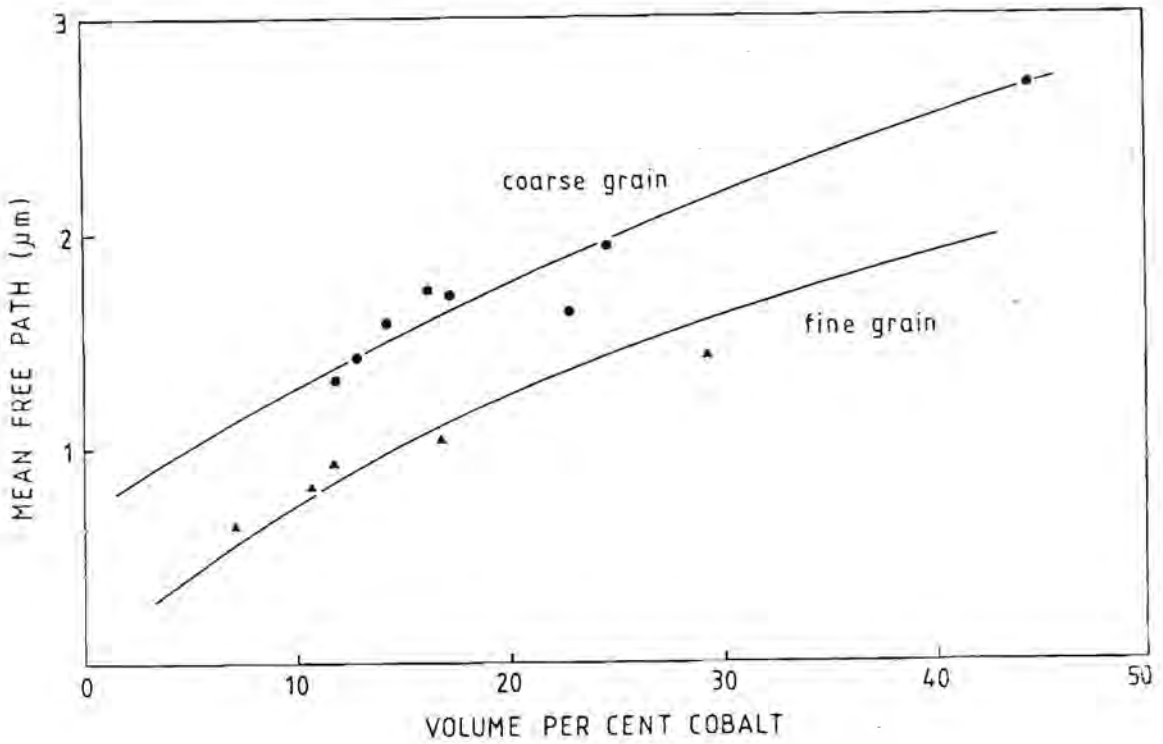

Figure 6.1 Mean free path as a function of experimental binder content and grain size with apparent trends indicated. ▲ = 1.8 μm, ● = 2.8 μm.

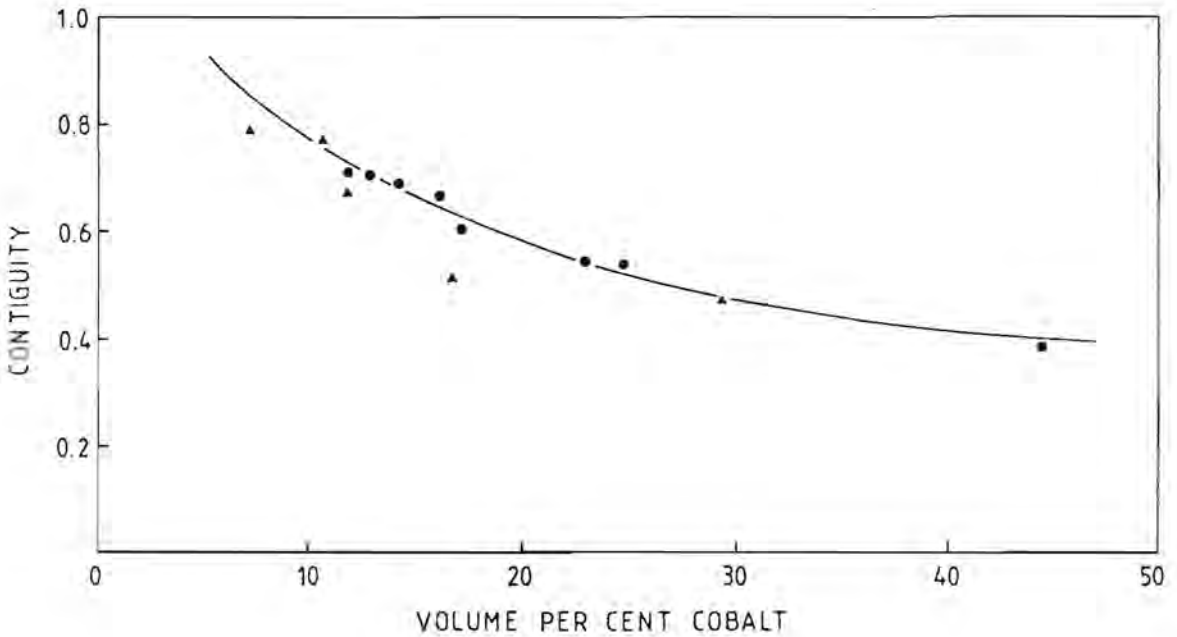

Figure 6.2: Contiguity as a function of experimental binder content and grain size with apparent trends indicated. ▲ = 1.8 μm, ● = 2.8 μm.

Table 6.2: Comparison of volume % binder for the WC-Co alloys

GRADE	DENSITY	VOLUME % COBALT		
	g/cm^3	EXPERIMENTAL	BOART	PENNEFATHER
A1	15.15	7.13	8.46	8.46
B1	14.92	10.55	10.08	11.68
B2	14.84	11.74	11.68	13.25
B3	14.51	16.64	16.33	22.23
B4	13.66	29.27	30.51	30.51
F1	14.84	11.74	10.08	11.68
F2	14.48	17.09	16.33	22.23
F3	13.98	24.52	23.66	23.66
G1	14.79	12.84	11.68	11.68
G2	14.68	14.12	13.25	14.80
G3	14.55	16.05	14.80	16.33
G4	14.10	22.73	19.32	22.23
I1	12.65	44.28	42.94	42.94
C1	14.98	9.66	10.08	8.46
C2	14.34	19.21	19.32	20.79
H1	14.66	14.41	13.25	13.25
H2	14.57	15.75	16.33	19.32
D1	15.02	9.06	10.08	10.08
E1	14.84	11.74	10.08	10.08

6.2 MECHANICAL PROPERTIES OF THE WC-Co ALLOYS INVESTIGATED

The experimental hardness values were found to be in agreement with those obtained by Pennefather. These, and the fracture toughness values determined by Pennefather, using the Palmqvist indentation method, are shown in Table 6.3.

Table 6.3: Hardness and fracture toughness of the WC-Co alloys

GRADE	HARDNESS (HV30)	FRACTURE TOUGHNESS (MPa $m^{1/2}$)
A1	1652	5.43
B1	1621	5.43
B2	1566	5.87
B3	1270	8.15
B4	1044	18.80
F1	1382	7.13
F2	1193	12.61
F3	1146	18.31
G1	1347	9.66
G2	1326	10.42
G3	1232	12.05
G4	1175	16.29
I1	716	-
C1	1516	6.00
C2	1231	16.08
H1	1245	12.64
H2	1193	15.44
D1	1678	5.73
E1	1800	5.00

6.2.1 Hardness

The hardness decreased with increased binder content and increased grain size as shown in fig. 6.3.

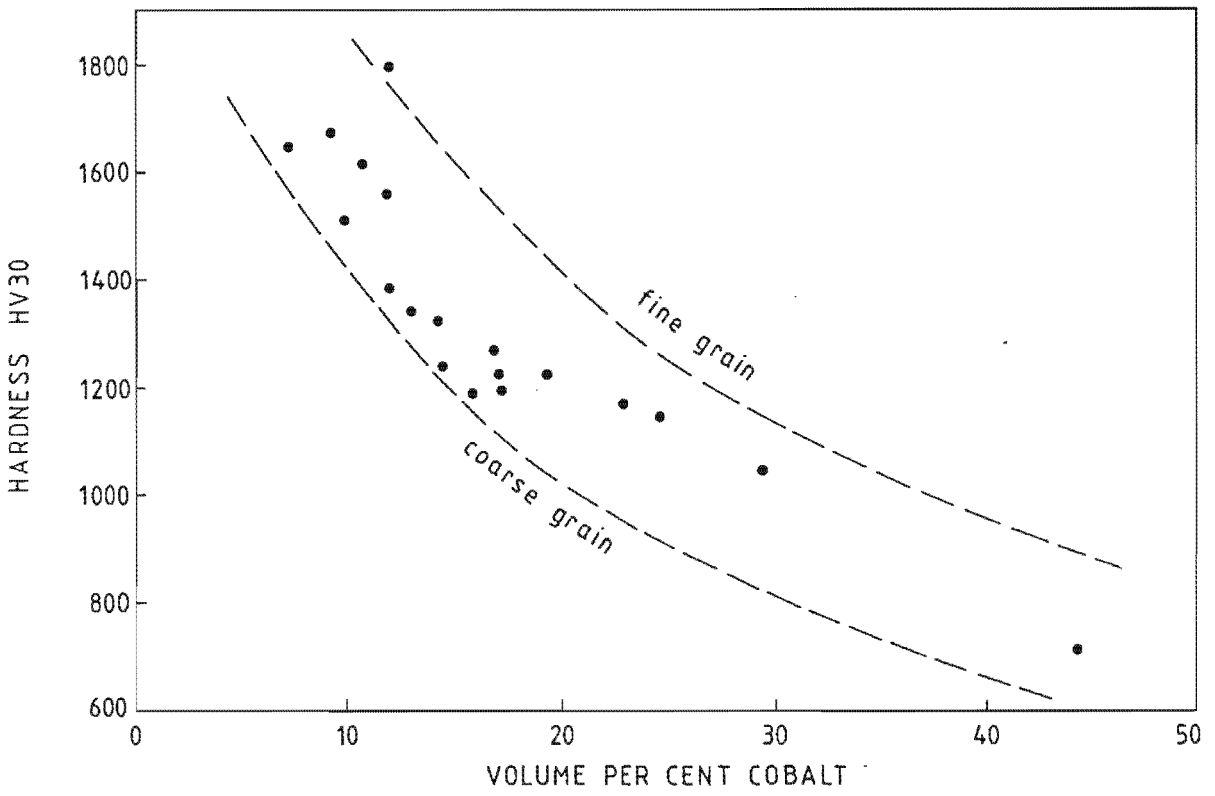

Figure 6.3: Variation of hardness with experimental binder content and grain size

6.2.2 Fracture Toughness

The dependence of fracture toughness on binder content and grain size is shown in fig 6.4. Fracture toughness increased with increased binder content and grain size. Fracture toughness decreased with increasing hardness as shown in fig. 6.5.

6.2.3 Youngs Modulus

The experimentally obtained values for Youngs modulus of the WC-Co alloys are given in Table 6.4.

Figure 6.5 shows the variation of Youngs modulus with binder content. The experimental values were in agreement with values reported by Doi et al (9), and Chermant et al (6). Theoretical curves for the upper and lower bounds are also shown. The outer bounds are the mixture formula bounds derived by Paul (in Doi et al (9)), while the inner bounds are the variational bounds calculated by Hashin and Shtrikman (in Doi et al (9)). The experimental values generally fall within both sets of bounds.

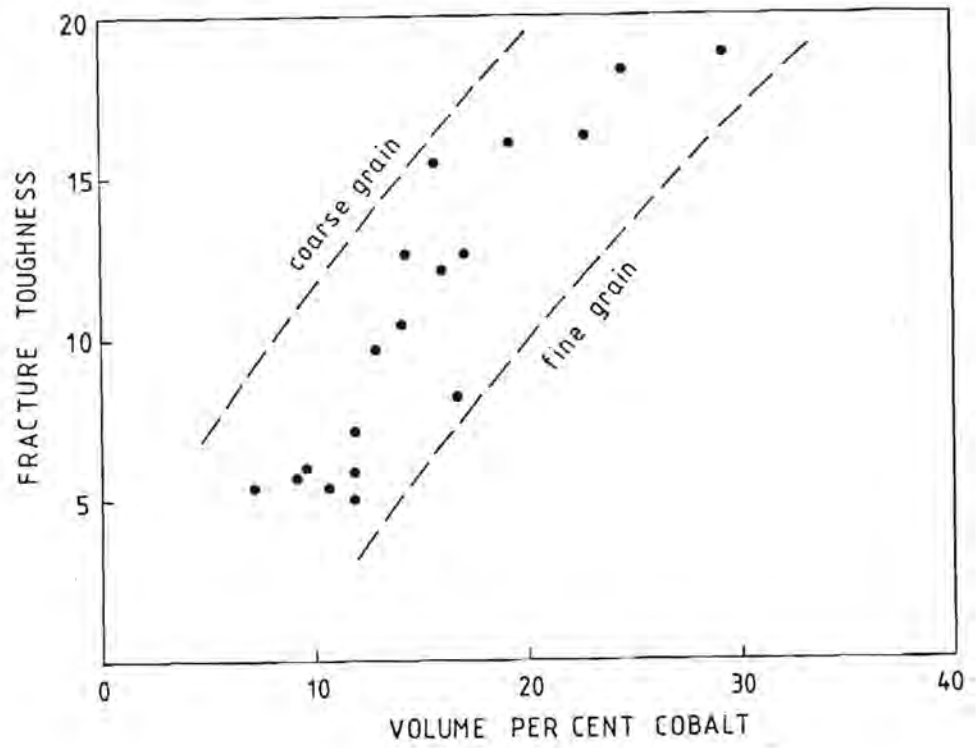

Figure 6.4: Fracture toughness of the WC-Co alloys as a function of experimental binder content and grain size.

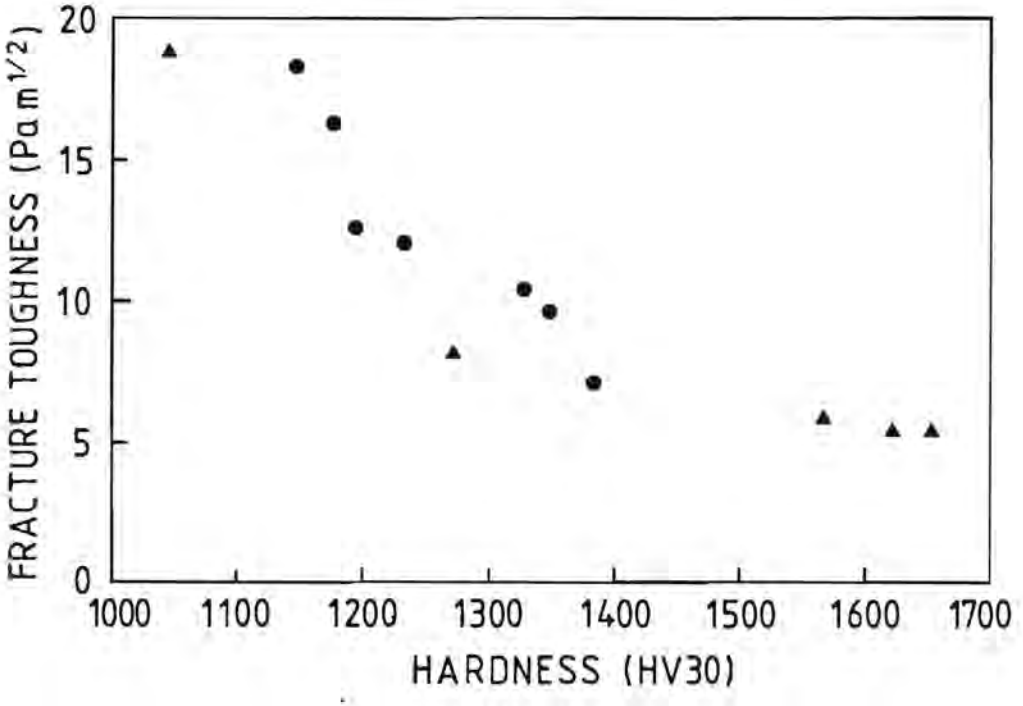

Figure 6.5: Dependence of fracture toughness on hardness for the 1.8 μm (▲) and 2.8 μm (●) grain sized grades.

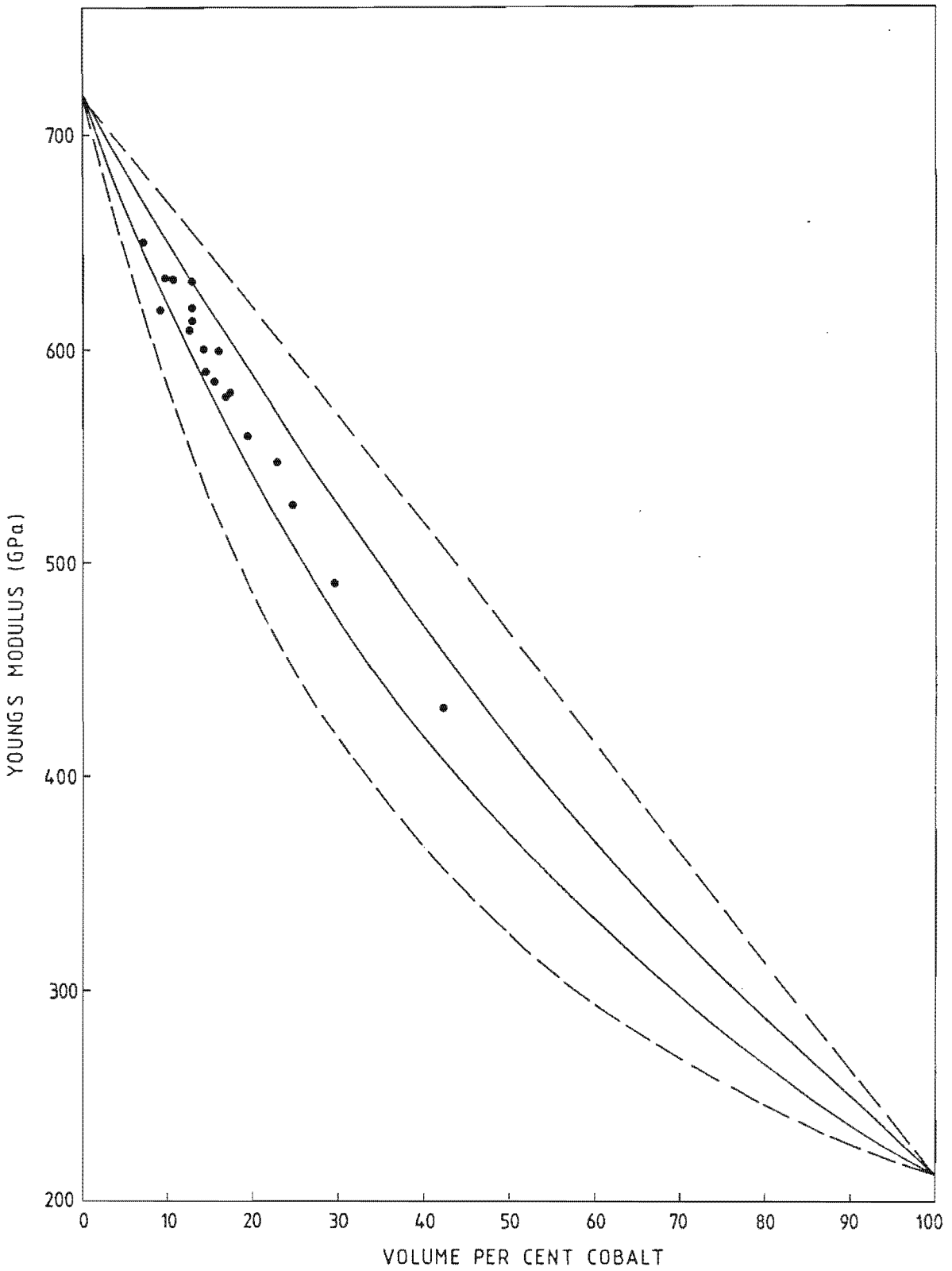

Figure 6.6: Variation of Youngs modulus of WC-Co with cobalt content, showing theoretical bounds.

Doi et al (9) found that in general, the elastic moduli do not depend on the tungsten carbide grain size. This is borne out by the experimental results, as shown in fig. 6.7 where only the 1.8 μm and 2.8 μm grain size are considered.

The dependence of Youngs modulus on contiguity is shown in fig. 6.8. There appears to be a change in the dependance as the contiguity increases. This change in slope occurs at a contiguity value of approximately 10 wt-% cobalt.

Table 6.4: Experimental values for Youngs modulus and Poissons ratio for the WC-Co alloys

GRADE	DENSITY (g/cm^3)	POISSONS RATIO	YOUNGS MODULUS (GPa)
A1	15.15	0.21	649.4
B1	14.92	0.21	633.0
B2	14.84	0.20	619.6
B3	14.51	0.21	579.3
B4	13.66	0.23	490.4
F1	14.84	0.21	624.8
F2	14.48	0.22	580.8
F3	13.98	0.22	528.3
G1	14.79	0.21	610.1
G2	14.68	0.21	602.8
G3	14.55	0.21	601.6
G4	14.10	0.22	549.9
I1	12.65	0.24	431.0
C1	14.98	0.20	634.2
C2	14.34	0.22	564.2
H1	14.66	0.21	587.5
H2	14.57	0.21	585.4
D1	15.02	0.21	617.8
E1	14.84	0.20	632.5

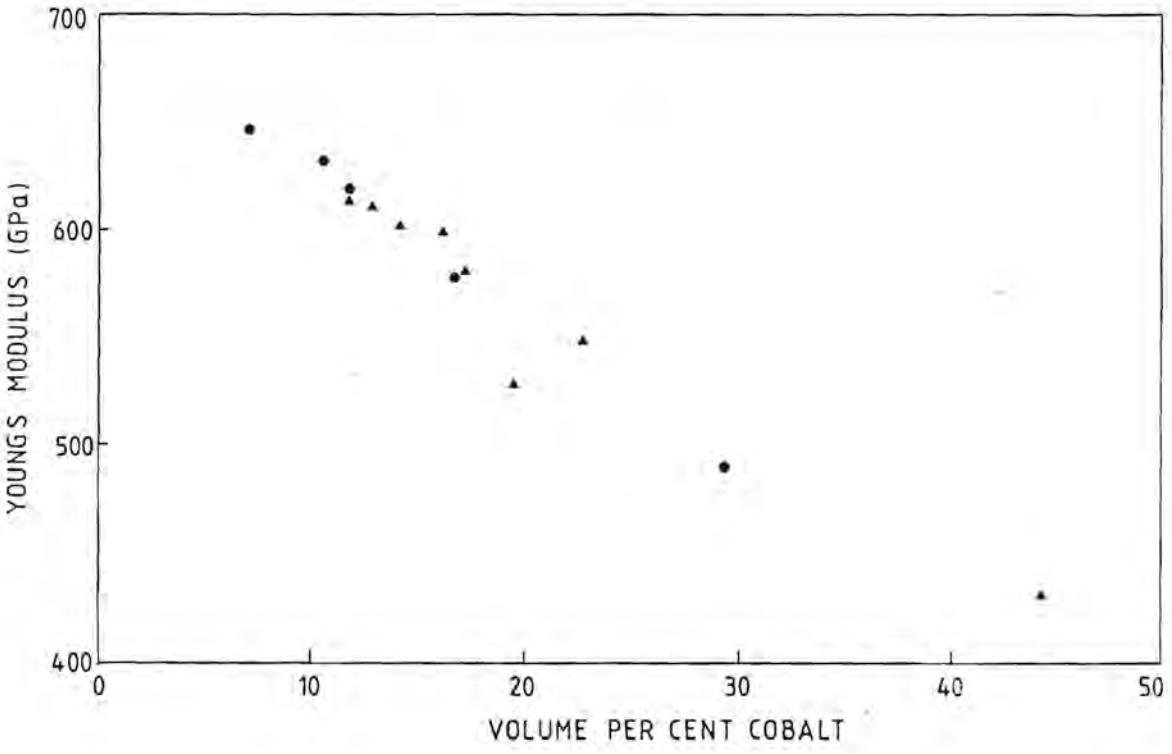

Figure 6.7: Variation of Youngs modulus of the WC-Co alloys with cobalt content. ▲ = 1.8 μm, ● = 2.8 μm.

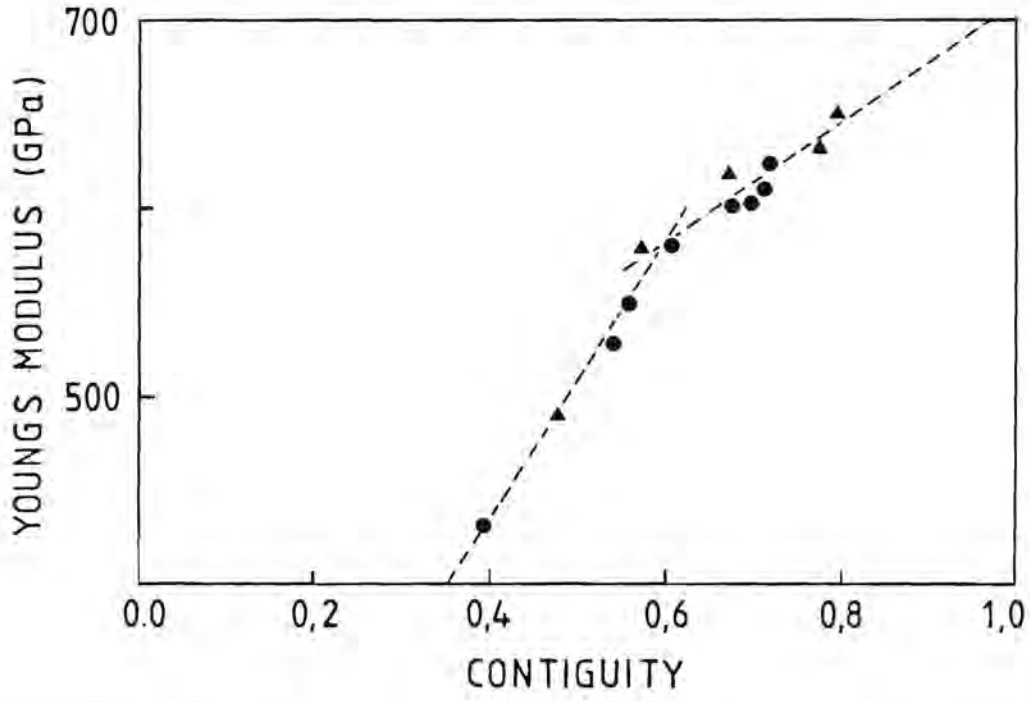

Figure 6.8: Variation of Youngs modulus with contiguity with apparent trends shown. ▲ = 1.8 μm, ● = 2.8 μm.

6.3 VIBRATORY CAVITATION EROSION

The vibratory cavitation erosion results and the microstructural parameters and mechanical properties are given in Table 6.5. The alloys were all tested a minimum of twice. The experimental scatter ± δ was calculated using:

$$\delta\,(\%) \;=\; 1/\bar{x} \sum_{n=1}^{n} (x-x_i)/n \;\bar{x}\; 100 \qquad (7.1)$$

where $\bar{x}$ is the average total CVL, x_i is the CVL of the ith test and n is the number of tests conducted. δ is thus the mean deviation expressed as a percentage of the average CVL. The average scatter was 8.56%.

6.3.1 Effect of Microstructure on Cavitation Erosion

Only those grades with grain sizes of 1.8 μm and 2.8 μm were considered when studying the effect of microstructure, due to the large variety in the range of alloys.

6.3.1.1 Binder Content

Figs. 6.9, 6.10 and 6.11 show the effect of volume percent binder on the five hour CVL, the erosion rate and t_0. Erosion rate and volume loss do not increase with increasing binder content as expected. Instead erosion reaches a maximum which is grain size dependent. For the smaller, 1.8 μm, grain size the maximum is at approximately 12 vol-% cobalt, whilst for the larger, 2.8 μm, grain size tne maximum is at approximately 23 vol-%. The incubation time decreases to a minimum at a binder content corresponding to the maximum in erosion rate.

6.3.1.2 Mean Free Path

Fig. 6.12 shows the effect of mean free path on the erosion of the 1.8 μm and 2.8 μm grain size grades. Both grain sizes pass through a maximum, but not at constant mean free path.

GRADE	GRAIN SIZE (μm)	VOLUME % COBALT	DENSITY (g/cm^3)	5 HOUR VOL LOSS cav (mm^3)	EROSION RATE cav (mm^3/h)	INCUB TIME cav (h)	5 HOUR VOL LOSS corr (mm^3)	MEAN FREE PATH (μm)	CONTIG-UITY	HARD-NESS (HV30)	FRACTURE TOUGHNESS ($MPam^{½}$)	YOUNGS MODULUS GPa
A1	1.46	7.13	15.15	0.387	0.105	1.30	0.012	0.642	0.790	1652	5.43	649.4
B1	1.85	10.55	14.92	0.508	0.134	1.20	0.015	0.810	0.773	1621	5.43	633.0
B2	1.88	11.74	14.84	0.903	0.203	0.55	0.008	0.927	0.670	1566	5.87	619.6
B3	1.78	16.64	14.51	0.581	0.150	1.13	0.009	1.024	0.570	1270	8.15	579.3
B4	1.76	29.27	13.66	0.364	0.113	1.78	0.012	1.436	0.475	1044	18.80	490.4
F1	2.98	11.74	14.84	0.073	0.038	3.10	0.005	1.317	0.715	1382	7.13	624.8
F2	2.83	17.09	14.48	0.396	0.104	1.17	0.021	1.729	0.604	1193	12.61	580.8
F3	2.85	24.52	13.98	0.397	0.116	1.58	0.021	1.950	0.540	1146	18.31	528.3
G1	2.80	12.84	14.79	0.153	0.051	1.97	0.005	1.425	0.710	1347	9.66	610.1
G2	2.64	14.12	14.68	0.251	0.073	1.55	0.005	1.581	0.694	1326	10.42	602.8
G3	2.82	16.05	14.55	0.302	0.106	2.15	0.008	1.740	0.673	1232	12.05	601.6
G4	2.58	22.73	14.10	0.736	0.199	1.29	0.021	1.637	0.556	1175	16.29	549.9
I1	2.17	44.28	12.65	0.100	0.066	3.48	0.015	2.690	0.392	716		431.0
C1	2.42	9.66	14.98	0.478	0.158	1.97	0.008	0.823	0.728	1516	6.00	634.2
C2	2.00	19.21	14.34	0.949	0.234	0.95	0.015	1.435	0.630	1231	16.08	564.2
H1	3.31	14.41	14.66	1.003	0.222	0.48	0.012	1.714	0.680	1245	12.64	587.5
H2	3.00	15.75	14.57	0.937	0.215	0.65	0.008	1.986	0.550	1193	15.44	585.4
D1	1.28	9.06	15.02	0.412	0.131	1.85	0.016	0.510	0.660	1678	5.73	617.8
E1	0.56	11.74	14.84	0.033	0.009	1.35	0.005	0.330	0.831	1800	5.00	632.5

Table 6.5: Cavitation erosion parameters, microstructural parameters and mechanical properties of WC-Co alloys.

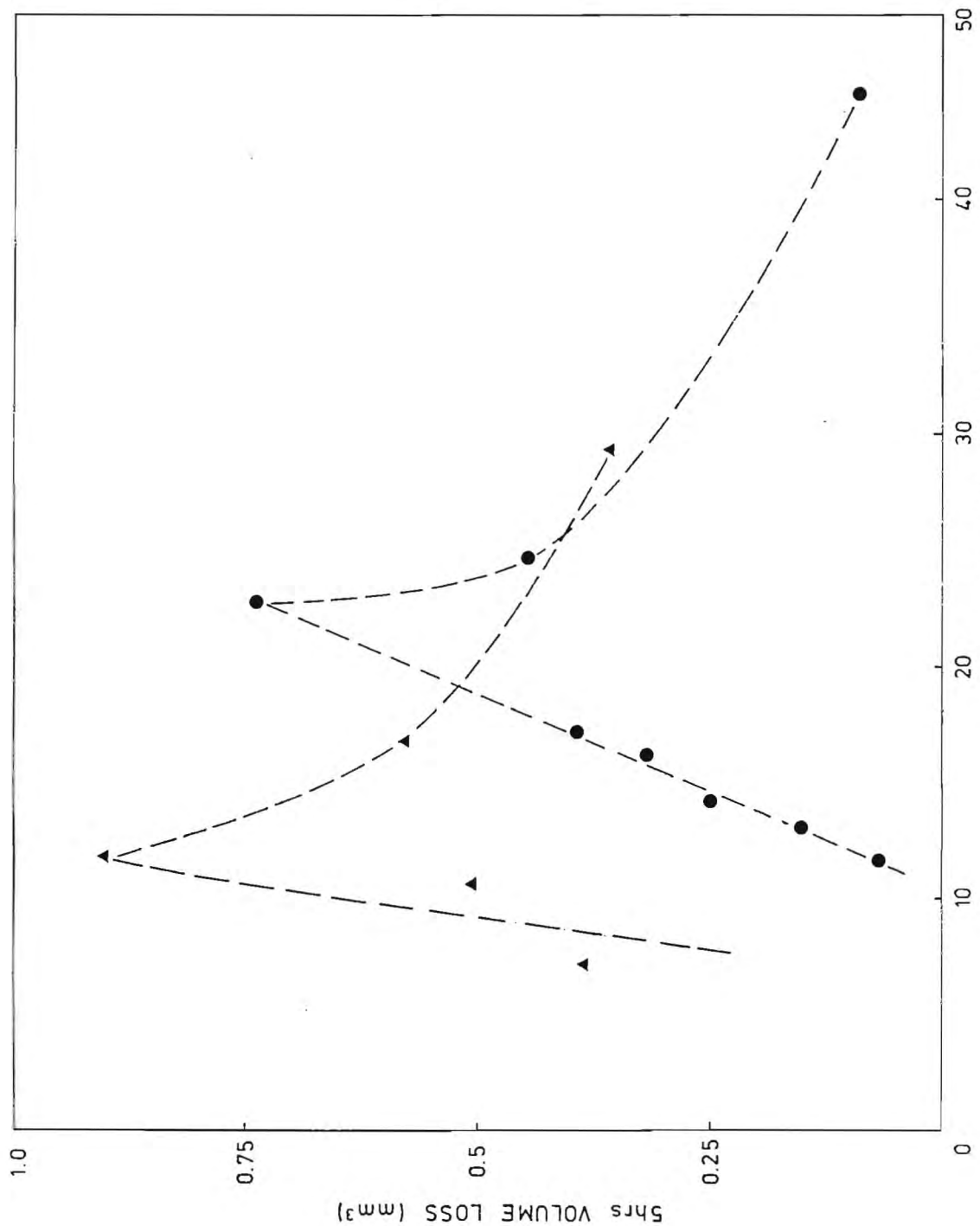

Figure 6.9: Cumulative volume loss as a function of binder content and grain size. ▲ = 1.8 μm grades, ● = 2.8 μm grades.

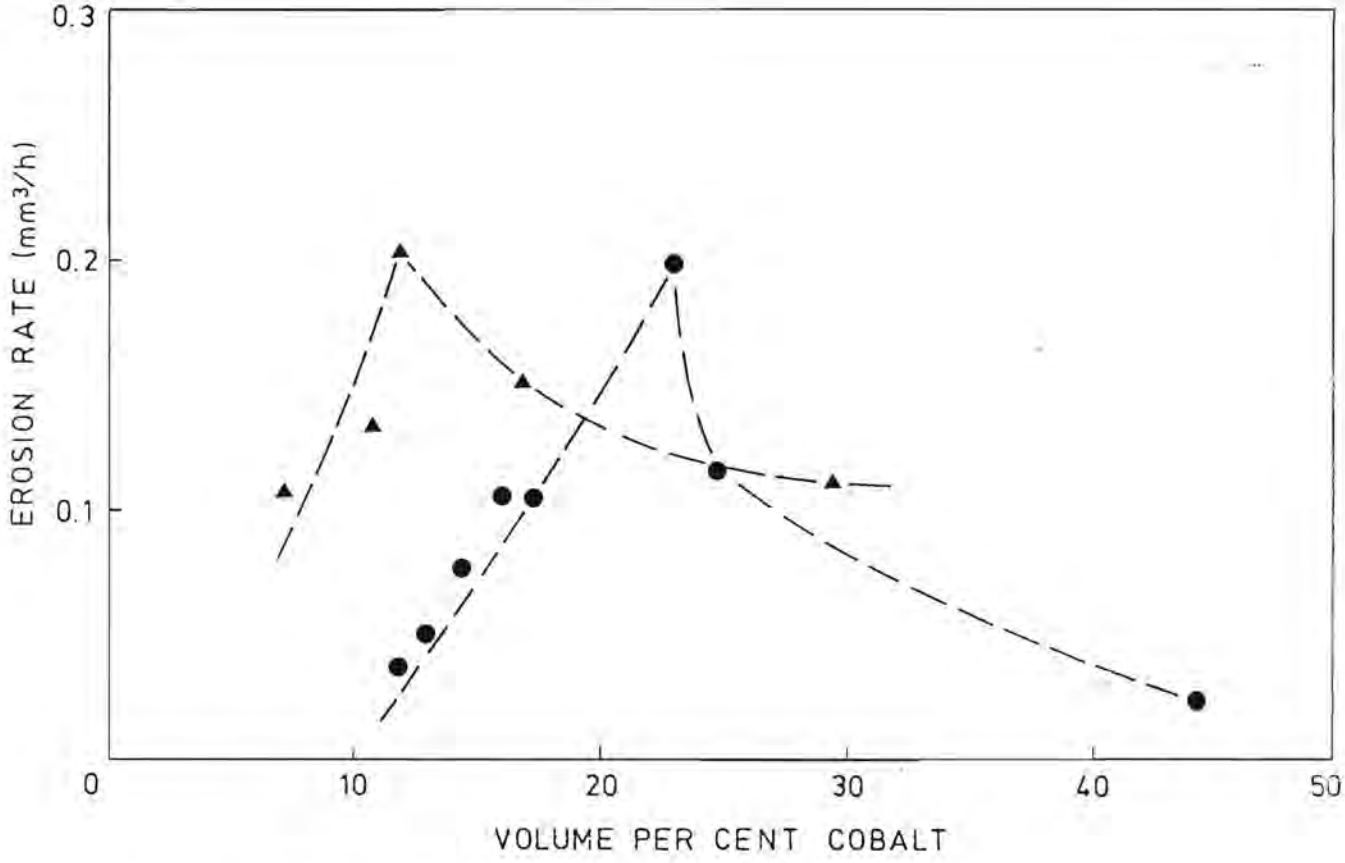

Figure 6.10: Erosion rate as a function of binder content and grain size. ▲ = 1.8 μm grades, ● = 2.8 μm grades.

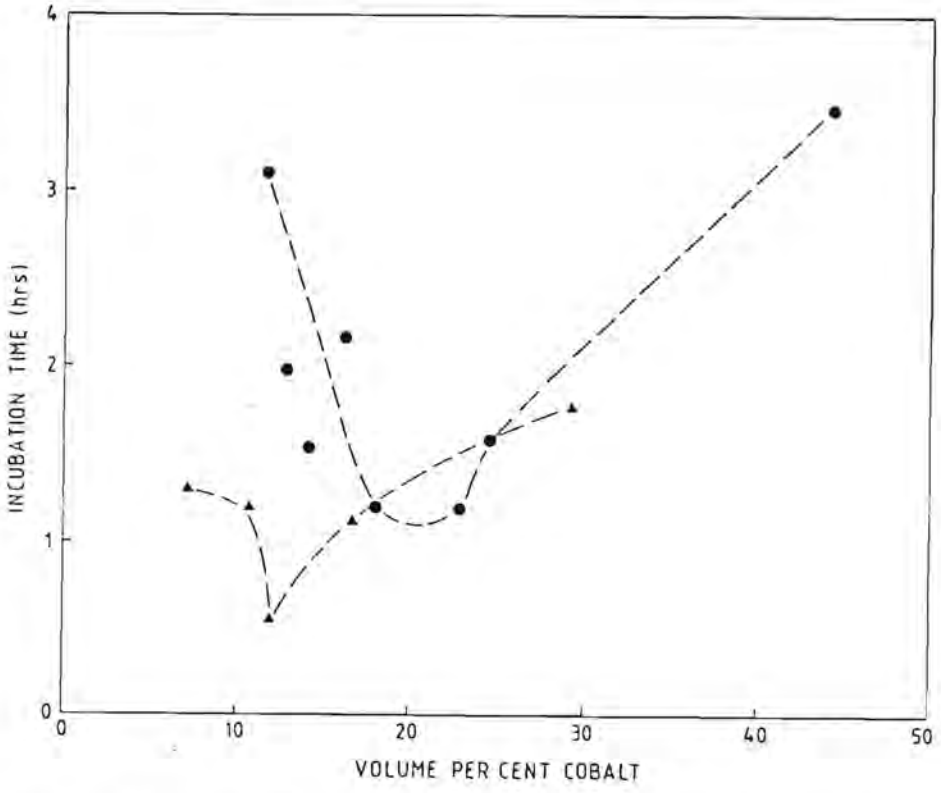

Figure 6.11: Incubation time as a function of binder content and grain size. ▲ = 1.8 μm grades, ● = 2.8 μm grades.

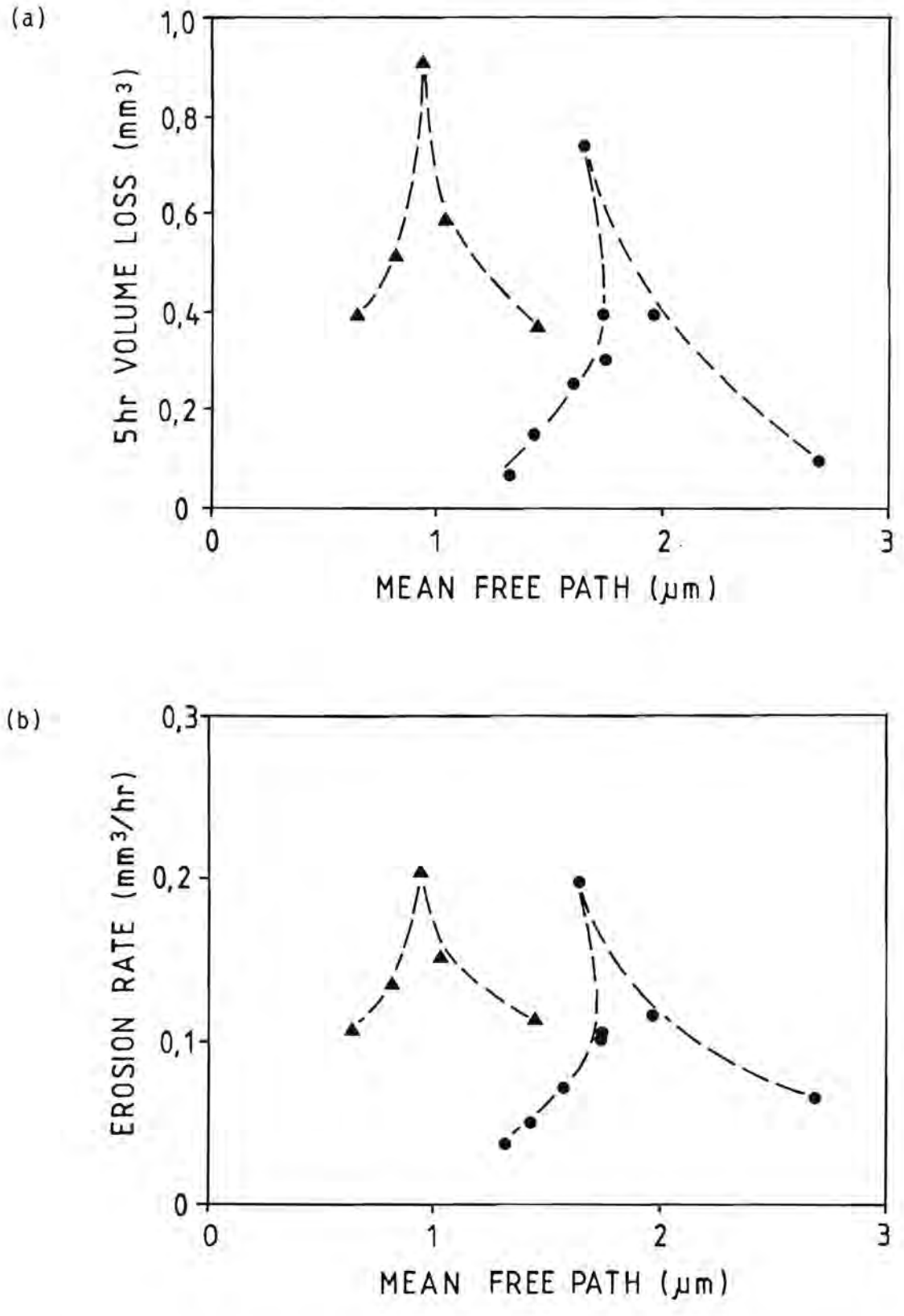

Figure 6.12: Dependence of a) cumulative volume loss and b) erosion rate on mean free path, for the 1.8 μm (▲) and 2.8 μm (●) grain sized samples.

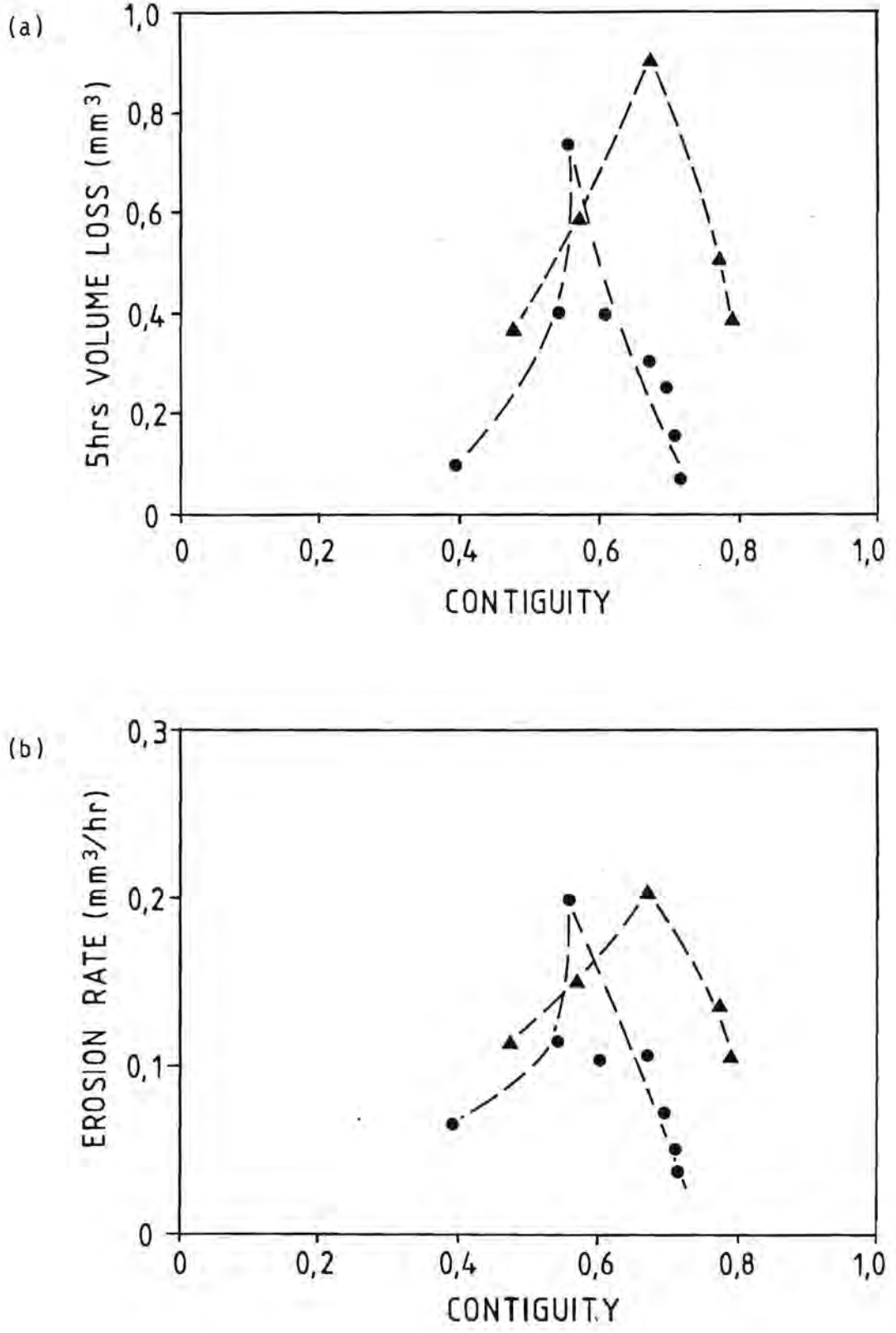

Figure 6.13: Dependence of a) cumulative volume loss and b) erosion rate on contiguity, for the 1.8 μm (△) and 2.8 μm (●) grain sized grades.

6.3.1.3 Contiguity

Erosion rate increases to a maximum as shown in fig. 6.13. The two grain sizes considered pass through a maximum, but at different values of contiguity. These values of contiguity correspond to the binder content where maximum erosion loss occurs (12 vol-% and 23 vol-% for the 1.8 μm and 2.8 μm grain size respectively).

6.3.1.4 Transformation of the Binder

The transformation of the binder during the course of a cavitation erosion test is shown in fig. 6.14. The amount of hcp cobalt increases rapidly during the initial part of the test and then levels off. In all the grades the amount of transformation reached its limit during the incubation period.

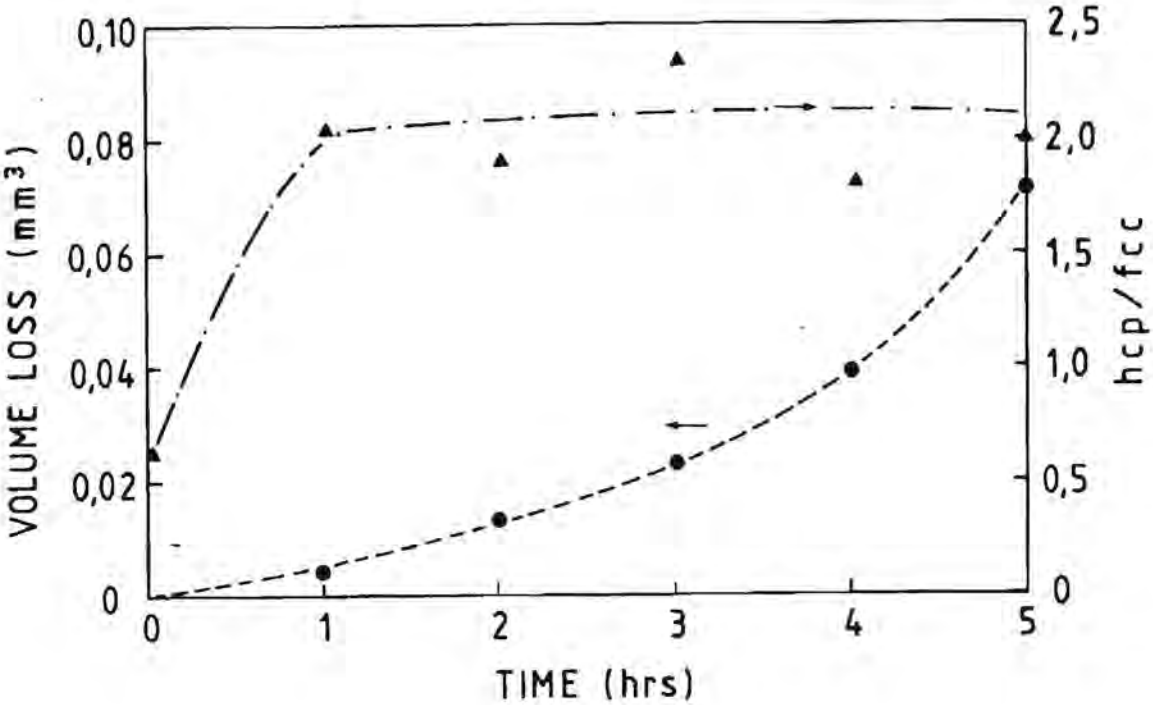

Figure 6.14: Cumulative volume loss and binder transformation versus exposure time for grade F1 (11.74 vol-%, 2.98 μm).

Fig. 6.15 shows the percentage transformation of the binder after five hours cavitation erosion as a function of the binder content. The percentage transformation increases with increasing cobalt content up to the binder contents associated with maximum erosion for both groups. Above these maxima the percentage transformation appears to level off at about 43% for the 1.8 μm and 70% for the 2.8 μm grain sized grades respectively. Of course the total amount of transformation increases because the volume percent of binder is increasing.

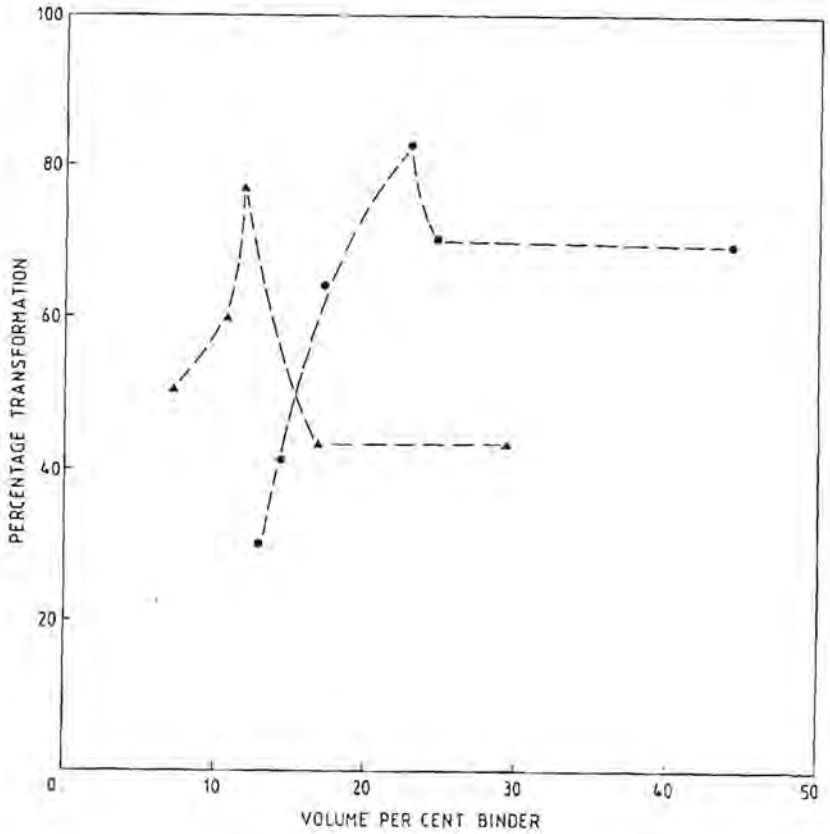

Figure 6.15: Percentage increase in transformation of binder during cavitation as a function of binder content (▲ = 1.8 μm, ● = 2.8 μm grain size).

6.3.2 The Dependence of Cavitation Erosion on Mechanical Properties

6.3.2.1 Hardness

Fig. 6.16 shows the dependence of erosion on hardness for the 1.8 μm and 2.8 μm grain sized grades. For each grain size, erosion increases with increasing hardness to a maximum. A further increase in hardness results in decreased erosion. The maxima relate to 12 vol-% cobalt for the 1.8 μm grain sized samples and 23 vol-% cobalt for the 2.8 μm grain sized samples. These are the binder contents which show maximum erosion for the respective grain sizes.

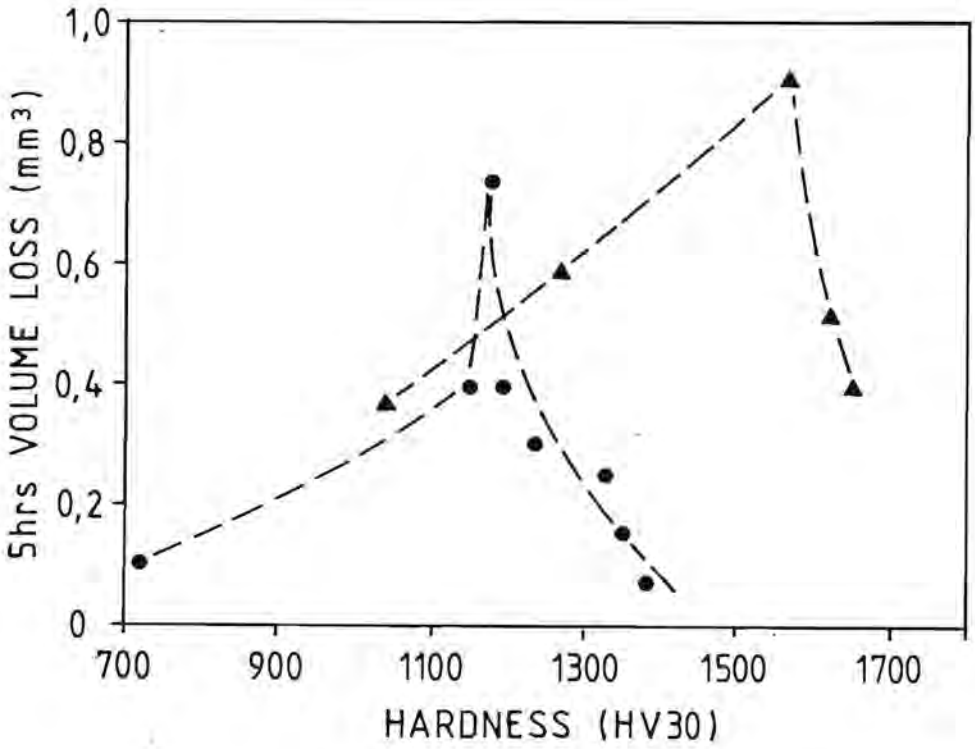

Figure 6.16a: The dependence of cumulative volume loss on hardness for the 1.8μm (▲) and 2.8μm (●) grain sized grades.

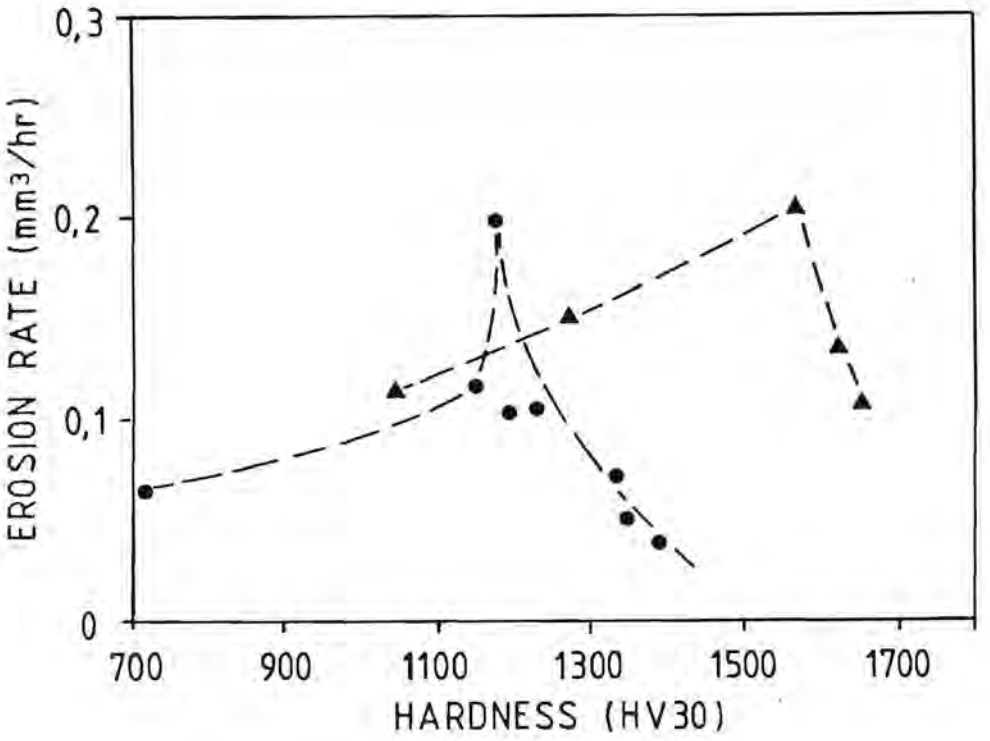

Figure 6.16b: The dependence of erosion rate on hardness for the 1.8 μm (▲) and 2.8 μm (●) grain sized grades.

6.3.2.2 Fracture Toughness

The dependence of erosion on fracture toughness is shown in fig. 6.17. Maximum erosion occurs at fracture toughness values relating to the binder contents giving maximum erosion (12 vol-% and 23 vol-% for the 1.8 μm and 2.8 μm grain sized grades respectively).

6.3.2.3 Youngs Modulus

Fig. 6.18 shows the dependence of erosion on Youngs modulus for the 1.8 μm and 2.8 μm grain sized grades respectively. Again, maximum erosion is found for values relating to 12 vol-% and 23 vol-% for the 1.8 μm and 2.8 μm grain sized grades respectively

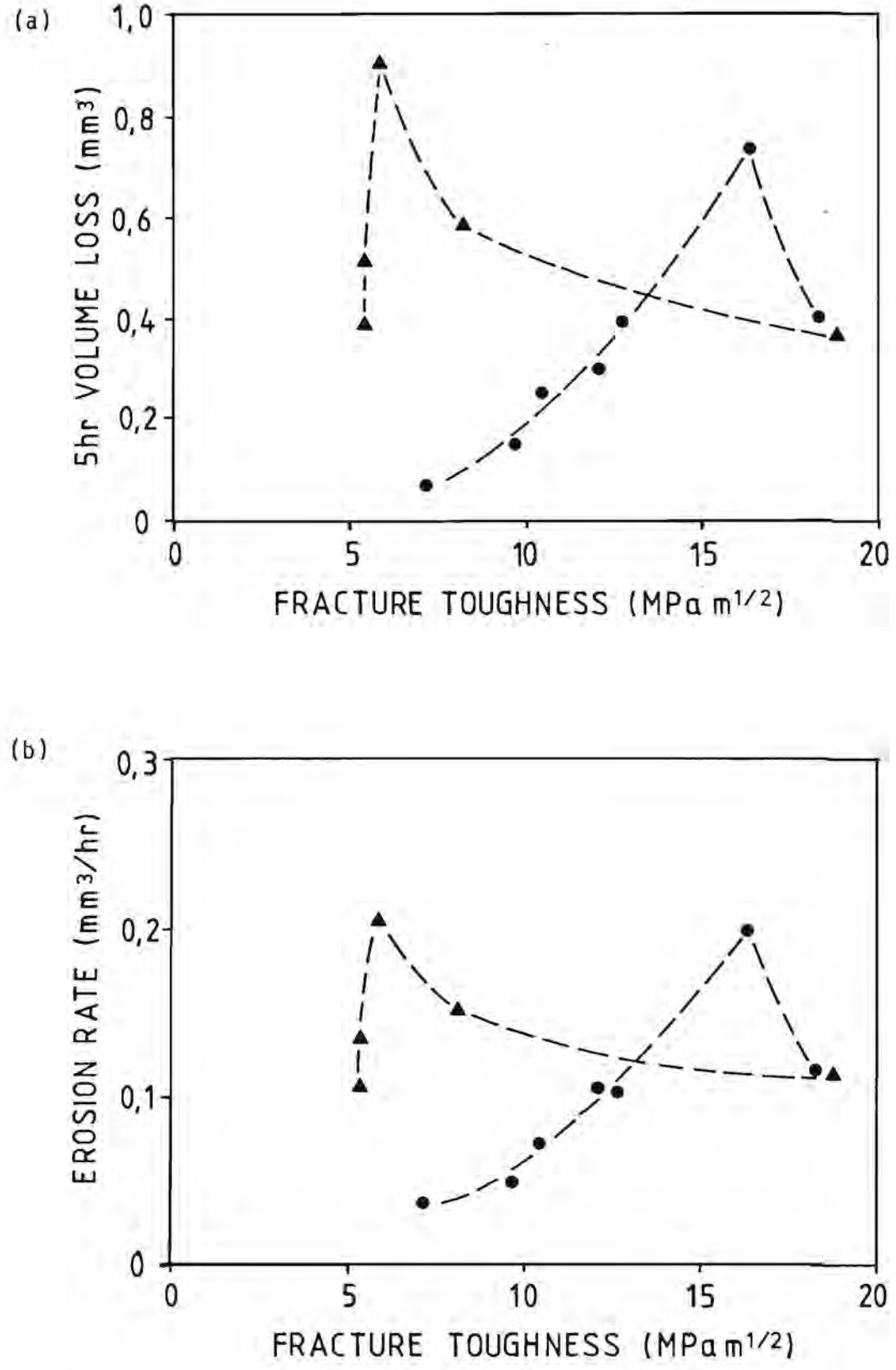

Figure 6.17: Dependence of a) cumulative volume loss and b) erosion rate on fracture toughness. ▲ = 1.8 μm grades, ● = 2.8 μm grades.

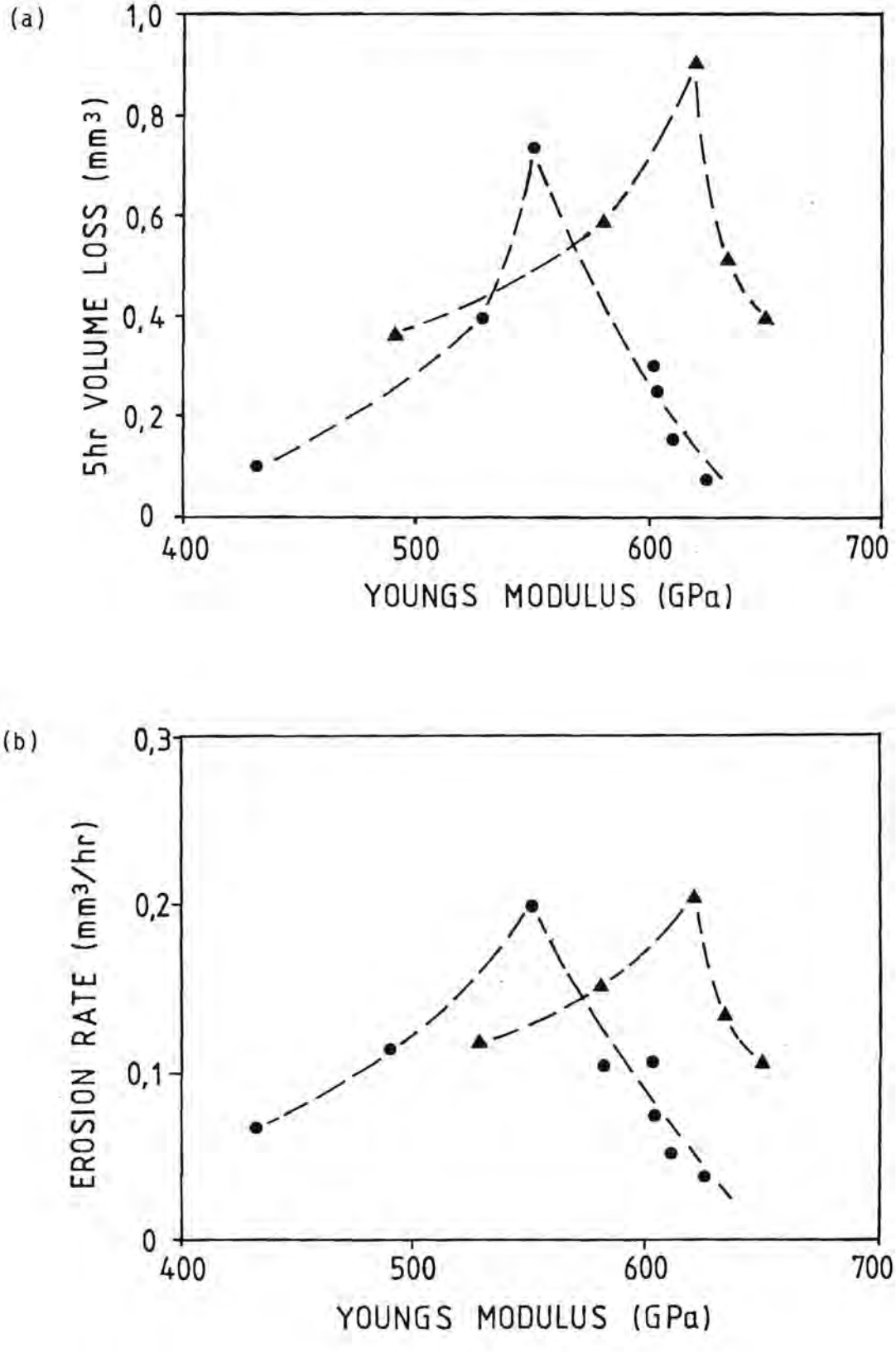

Figure 6.18: Dependence of a) cumulative volume loss and b) erosion rate on Youngs modulus. ▲ = 1.8 μm grades, ● = 2.8 μm grades.

6.3.3 CORROSION EFFECTS

In order to determine any possible effect of corrosion on the cavitation erosion of the WC-Co alloys, the volume loss sustained by the dummy sample in the test bath was subtracted from that of the cavitation erosion sample as shown in fig. 6.19. Although corrosion was found to occur, its effect on the cavitation erosion was found to be negligible.

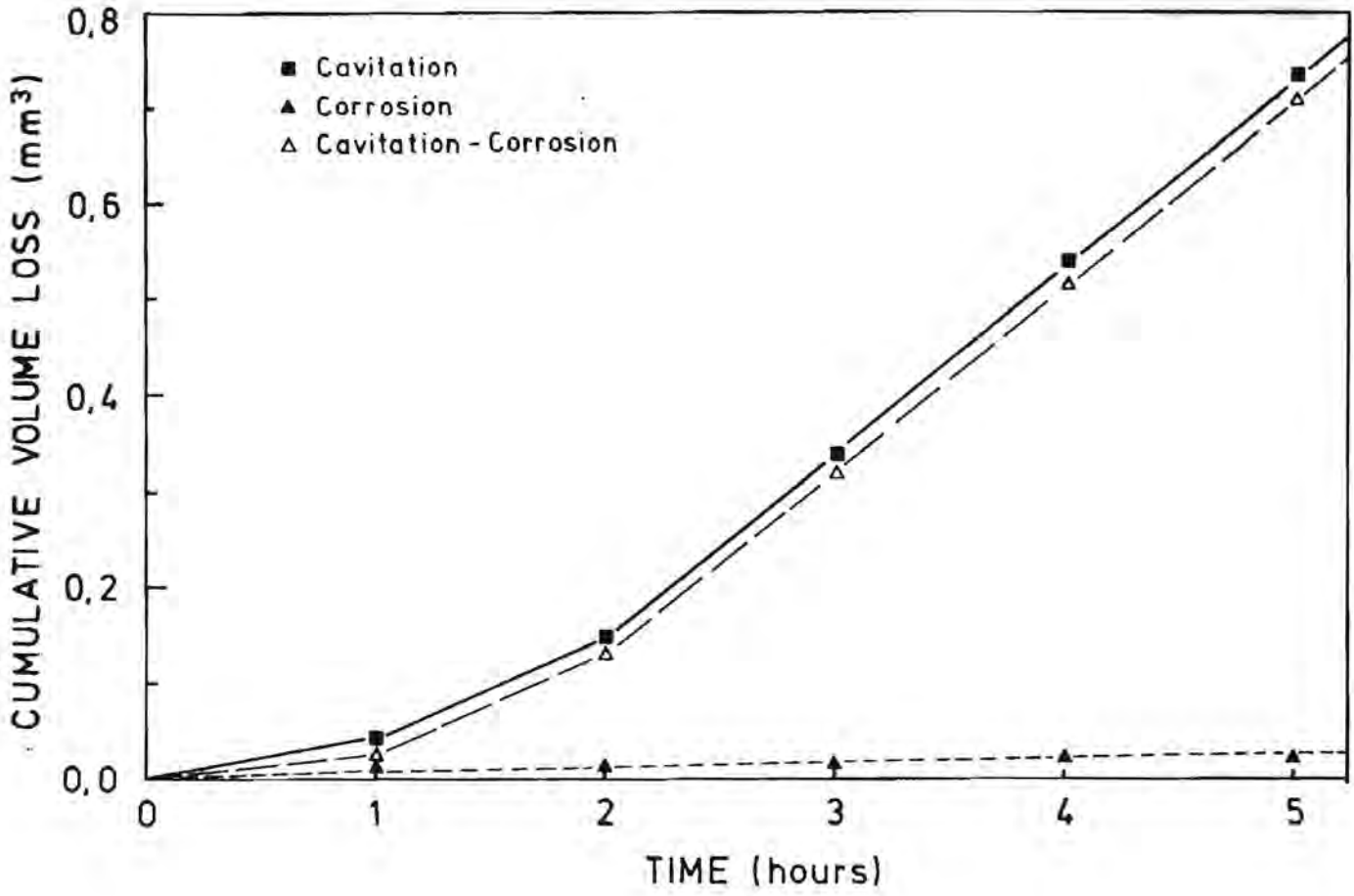

Figure 6.19: The effect of corrosion on cavitation erosion of grade G4 (22.73 vol-%, 2.58 μm).

Fig. 6.20, a scanning electron micrograph of corroded I1 , shows evidence of cobalt removal both at interfaces and in the bulk matrix. Pits such as these, if formed on cavitation samples, could act as wave guides for cavitation attack and result in an increase in erosion loss. For most of the grades, however, the corrosion loss was less than the experimental scatter for cavitation erosion loss.

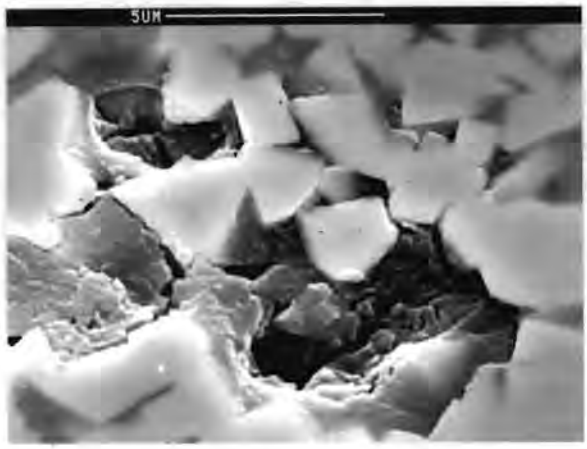

Figure 6.20: Scanning alectron micrograph of grade I1 (44 vol-%, 2.17 μm) after five hours in the test bath.

6.4 SCANNING ELECTRON MICROSCOPY

The mode of material removal during cavitation erosion was followed using scanning electron microscopy. For all the grades, regardless of binder content or grain size, cobalt removal was the initial step, as shown in fig. 21. In high binder grades (fig. 6.21a), cobalt removal was initiated both at carbide-cobalt interfaces and in the bulk cobalt. Cobalt removal is not uniform across the surface; preferential removal occurs by growth of the initial pits formed.

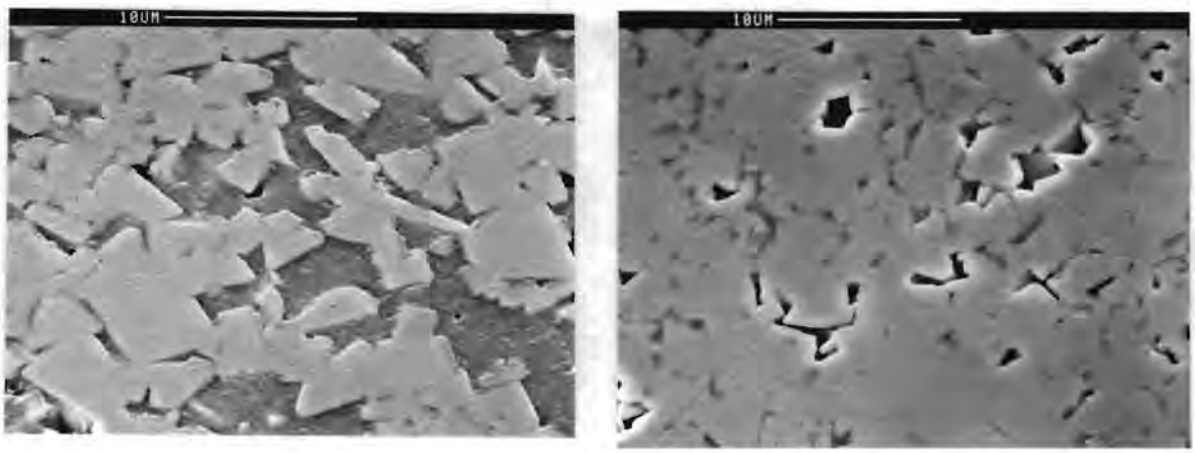

(a) (b)

Figure 6.21: Scanning electron micrographs of grades (a) I1 (44 vol-%, 2.17 μm) and (b) G2 (14 vol-%, 2.64 μm) after 15 minutes exposure to cavitation.

During the incubation period, cobalt removal is responsible for most of the material loss, especially in the high binder content grades, as shown in fig. 6.22a. Although large amounts of cobalt have been removed, the WC grains are still firmly embedded. For the lower binder content grades (figs. 6.22b and c) there is evidence of some WC loss. Preferential removal from already developed pits still occurs (fig. 6.22b) leaving the remaining skeleton essentially intact.

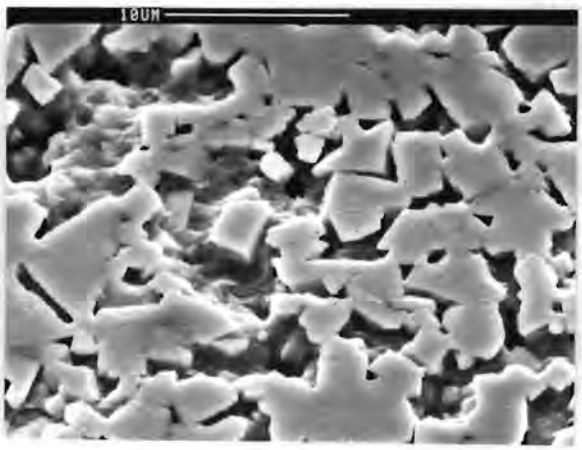

(a)

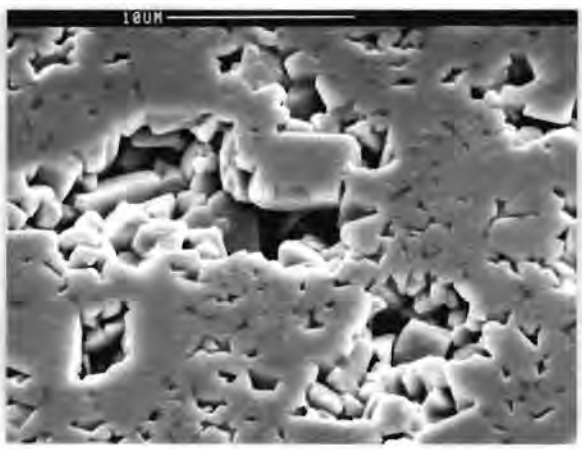

(b)

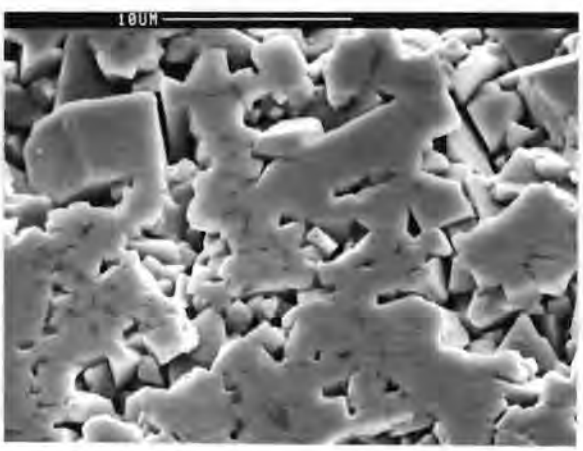

(c)

Figure 6.22: Scanning electron micrographs of grades (a) I1 (44 vol-%, 2.17 μm), (b) G3 (16 vol-%, 2.82 μm) and (c) G2 (14 vol-%, 2.64 μm) after one hour exposure to cavitation.

During steady state erosion, WC grain pull-out becomes more important. For high binder grades (fig. 6.23a) the continual removal of cobalt undermines the grains, essentially releasing them as individual grains. Contiguous carbide grains, however, remain bound together, while deep "worm holes" are formed in the surrounding matrix. For lower binder content (fig 6.23b) most of the surface cobalt has been removed and WC grain pull-out is more evident. The grains are still firmly packed and most material loss comes from established regions of damage.

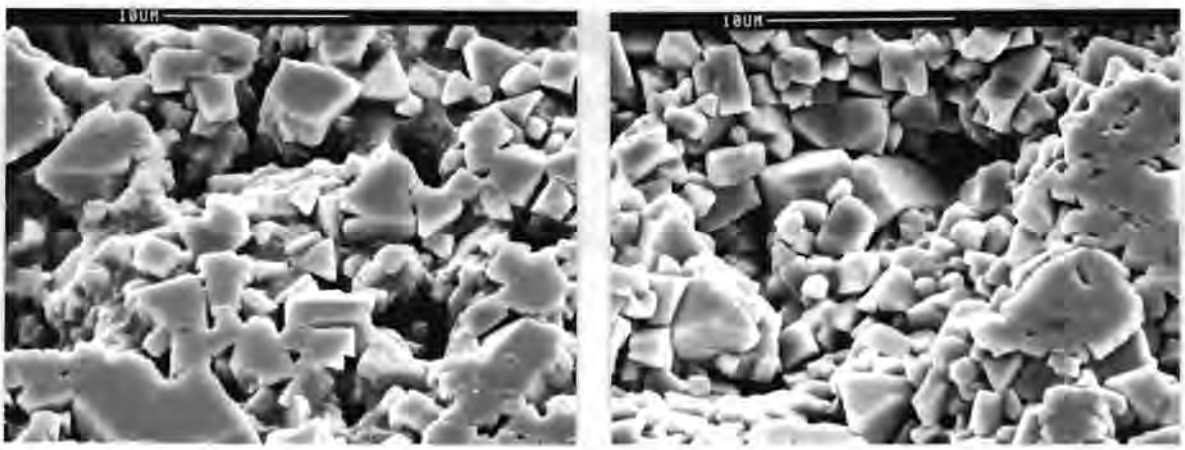

(a) (b)

Figure 6.23: Scanning electron micrographs of grades (a) I1 (44 vol-%, 2.17 μm) and (b) G3 (16 vol-%, 2.82 μm) after 5 hours exposure to cavitation.

The carbide skeleton remains fairly intact even during steady state erosion. In fig. 6.24a extensive removal of cobalt has occurred, but the WC grains are "stuck" together in regions surrounding areas of grain loss. The same effect is shown in fig. 6.24b where the larger grain size infers greater contiguity. Removal of cobalt from between the contiguous grains has begun, which will result in undermining and removal of the grains and the breakup of continuous aggregates of grains. Grain fracture was not observed during the cavitation erosion tests for any of the specimens tested irrespective of cobalt content or grain size.

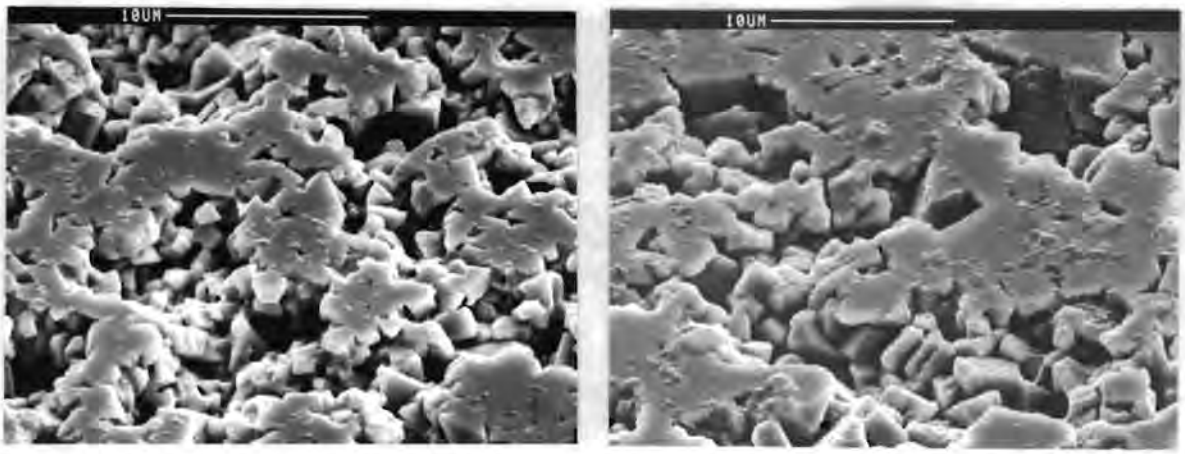

(a) (b)

Figure 6.24: Scanning electron micrographs of grades (a) B4 (29 vol-%, 1.76 μm) and (b) G4 (23 vol-%, 2.58 μm) during steady state erosion.

The scanning electron microscopy showed that the initial step in material removal during cavitation erosion was cobalt removal. As cobalt removal was predominant during the incubation period for all the alloys tested, it might be more relevant to use the density of cobalt, rather than the bulk density, to calculate the volume loss during this period. During steady state, however, both cobalt and WC are lost and using the bulk density would give a better approximation of the volume loss incurred. Thus erosion rate, which is a measure of steady state, is a better comparative measure of the erosion resistance of the alloys than five hour volume loss which includes the loss during the incubation period.

CHAPTER 7

DISCUSSION

7.1 MICROSTRUCTURE AND ITS EFFECT ON CAVITATION EROSION

All the microstructural parameters were found to affect the cavitation erosion of the alloys (figs. 6.9 to 6.13). For both mean free path and contiguity, maximum erosion occurred at values related to 12 vol-% and 23 vol-% for the 1.8 μm and 2.8 μm grain sized grades respectively.

Erosion rate would be expected to:

(i) increase with increasing binder content and hence mean free path. As the mean free path increases, the plastic constraint of the cobalt is reduced, leading to a reduction in hardness of the matrix and thus the alloy. This would reduce the erosion resistance of the alloy.

(ii) decrease with increased contiguity. If the WC skeleton is instrumental in resisting the cavitational forces, then a more rigid skeleton would confer greater erosion resistance. A fragile and discontinuous skeleton (low contiguity) is not able to withstand the cavitational forces, resulting in a high erosion rate.

Predictions (i) and (ii) above were found to be valid for alloys with binder contents of less than 12 vol-% (1.8 m grades) and 23 vol-% (2.8 m grades) (figs. 6.12, 6.13). For alloys with greater cobalt contents than these, the erosion rate decreased with increased mean free path and decreased contiguity (both equivalent to increased binder content). Some other process of absorbing strain becomes responsible for the erosion resistance shown by these alloys.

The transformation of the binder from the metastable fcc phase to the hcp phase seems to play a role in the erosion of the alloys (fig. 6.15).

Above 23 vol-% binder (2.8 μm grain sized grades) the percentage binder undergoing transformation during steady state erosion is approximately 70%. Thus as the binder content increases, the total strain accommodated by the cobalt transformation increases, since larger volumes of binder now undergo transformation. The levelling off at 70% is presumed (41)' to represent the critical fraction of transformation prior to local fracture and particle separation (debonding at cobalt-carbide interfaces) to occur.

For low binder content alloys only a small percentage of the binder transforms. The amount increases with increasing cobalt content and mean free path. It seems that plastic constraint of the binder associated with a small mean free path retards transformation by hindering the associated volume change. Transformation of the binder would thus play a limited role in accommodating strain from cavitation for low cobalt content alloys.

The slightly higher amount of transformation undergone by grades B2 (12 vol-%, 1.88 μm) and G4 (23 vol-%, 2.58 μm) might cause increased debonding at the carbide-cobalt interfaces, thus increasing the erosion rate despite any strain accommodation. The cobalt adhering to the exposed WC grains in fig. 6.24b might be evidence of such decohesion, but cannot be considered conclusive.

7.2 MECHANICAL PROPERTIES AND THEIR EFFECT ON CAVITATION EROSION

Hardness decreases with increasing binder content (fig. 6.3). This can be ascribed to two effects: the decrease in the amount of the harder phase (tungsten carbide), and the decreased plastic constraint of the binder. As the amount of binder increases, the mean free path increases, resulting in a reduction of the plastic constraint of the cobalt. This lowers the hardness of the binder and leads to a general decrease in the hardness of the alloy. An increase in grain size is associated with an increase in mean free path and hence a decrease in hardness.

It is expected that an increase in hardness would result in decreased erosion of the WC-Co alloys. This is true (fig. 6.16) for alloys with hardnesses greater than 1566 HV30 and 1175 HV30 for the 1.8 μm and 2.8 μm grain sized grades respectively. These hardnesses correspond to binder contents of less than 12 vol-% and 23 vol-% respectively. This suggests that for these binder contents the erosion is hardness related. For alloys with hardnesses less than 1566 HV30 (1.8 μm) or 1175 HV30 (2.8 μm), erosion decreases with decreasing hardness. This suggests that the erosion of higher binder content alloys is controlled by some property other than hardness.

The increased fracture toughness with increasing cobalt content (fig. 6.4) due to the higher toughness value of cobalt with respect to tungsten carbide. The crack blunting potential of cobalt is sufficient to limit cleavage of carbide grains. Larger carbide grains, however, are susceptible to transgranular fracture, which leads to a decrease in fracture toughness with increased grain size.

In the model established by Murray (19), fracture toughness is shown to be indirectly dependent on the hardness of the material as a whole, which varies with mean free path and grain size. Murray showed that the plastic zone at the crack tip is confined to a size equal to the mean free path, due to spatial constraints imposed by adjacent carbide particles. Leuth (23) found that the fracture toughess of WC-Co alloys is strongly dependent on mean free path and generally increases with increased mean free path. Thus as the binder content (and hence the mean free path) increases, the fracture toughness of the material increases.

As noted in section 6.2.3, the Youngs modulus of the alloys decreased with increasing binder content. The dependence of Youngs modulus on contiguity is seen to change at a value of approximately 0.6 (fig. 6.8). This contiguity is associated with a binder content of approximately 16 vol-%, which is the value at which a change in structure from a WC skeleton to embedded WC grains is thought to occur. Chermant et al (5) noted that the upper bound model of a dispersion of a ductile phase in a harder phase is valid for alloys with binder contents of less than 16 vol-% (approximately 10 wt-%). For alloys with more than 16 vol-% Co the lower bound model, corresponding to a dispersion of a harder phase in a ductile phase, was found to be valid.

The inflection in the curve in fig. 6.8 corresponds to this transition from a continuous WC skeleton which carries the applied stress, to the "embedded" structure where the given stress is distributed uniformly throughout the volume of the specimen, but the strain is predominantly in the matrix. The regression curves drawn in fig. 6.8 extrapolate to give Youngs modulus values of 709 GPa for WC and 197 GPa for Co. These values are slightly lower than the values given in Doi et al (9) (719 GPa for WC and 211 GPa for Co), but were considered acceptable.

Maximum erosion loss of the 1.8 μm and 2.8 μm grain sized grades occurs at values of hardness, fracture toughness and Youngs modulus relating to 12 vol-% and 23 vol-% respectively. These binder contents seem to represent the worst combination of microstructural and mechanical properties with regard to erosion resistance.

7.3 MODES OF MATERIAL REMOVAL

The scanning electron microscopy studies (section 6.4) showed that material removal, regardless of binder content and WC grain size, always followed the same trend. Cobalt is the initial step, which results in the undermining of WC grains. Grain removal only occurs when enough of the binder has been lost. Although cobalt removal was seen to initiate at carbide-cobalt interfaces (fig. 6.21), evidence of debonding as suggested by Heathcock (16) was only observed in grade G4 (23 vol-%, 2.58 μm) (fig. 6.24).

7.4 MODEL OF THE EROSION MECHANISM

Fig. 7.1 is a schematic summary of the model used to describe the mechanism of cavitation erosion of WC-Co alloys. For simplicity's sake only the 2,8 μm grain sized grades will be considered.

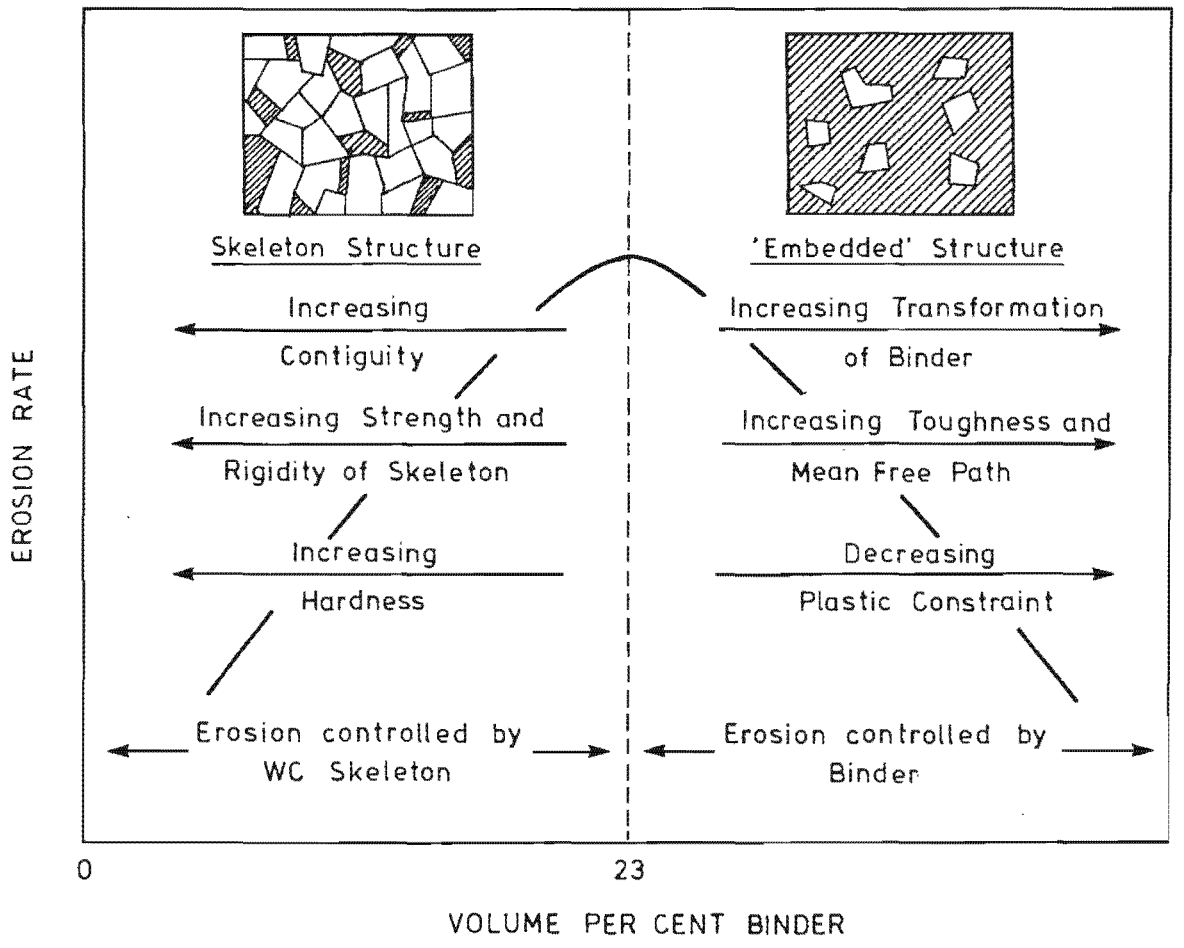

Figure 7.1: A schematic summary of cavitation erosion of 2.8 μm grain sized WC-Co alloys. The parameters believed to affect erosion are indicated.

The model can be divided into two sections: alloys containing more than 23 vol-% cobalt and alloys containing less than 23 vol-% cobalt.

7.4.1 WC-Co Alloys Containing More Than 23 Vol-% Cobalt

Cobalt removal is responsible for most of the material loss in these alloys (figs. 6.22a, 6.23a). The WC grains are essentially "embedded" in the binder and large amounts of cobalt must be removed before WC grains become "unbound" and are lost from the surface. The total strain absorbed by the transformation of the binder

increases with increasing binder content (section 7.1), thus reducing the erosion rate. The contiguity of these alloys is low and the WC skeleton is too discontinuous for it to have any noticeable effect on erosion resistance. It should be noted (fig. 6.23a) that isolated WC grains are lost during steady state in preference to contiguous grains. The toughness of the alloys increases with increasing binder content. This too would improve the erosion resistance of the alloys. The binder thus plays the controlling role in the erosion resistance of the high cobalt content alloys.

7.4.2 WC-Co Alloys Containing Less Than 23 Vol-% Cobalt

Although cobalt removal is the initial stage in the erosion of these alloys (fig. 6.21b), WC grain pullout is responsible for the majority of material loss (fig. 6.23b). The contiguity of the WC grains is essentially preserved even after most of the surface binder has been removed (fig 6.23b). For low binder content alloys this results in limited WC grain loss and thus good erosion resistance. The small mean free path associated with low binder content alloys results in high plastic constraint of the binder. This hardens the binder and retards the transformation of the binder. Thus for low cobalt content alloys the erosion is controlled by the WC skeleton. As the binder content increases, the contiguity decreases, weakening the WC skeleton. The associated increase in mean free path reduces the plastic constraint of the binder, reducing the hardness and the erosion resistance of the alloy. The maximum in erosion loss is thus associated with a fragile skeleton of WC and a matrix which has little capacity to absorb strain and resist microfracture.

CHAPTER 8

CONCLUSIONS

Previous microstructural characterisation of the WC-Co alloys by Pennefather (28) indicated that the majority of the alloys could be divided into two groups according to grain size. Since microstructure was seen to play an important role in the cavitation erosion of the WC-Co alloys, attention was focussed on these two groups of alloys. The following conclusions can be drawn from the investigation:

1. Mean free path, contiguity, grain size and binder content were all found to influence the cavitation erosion of the WC-Co alloys. Maximum erosion was observed at different binder contents, depending on grain size.

2. Cobalt removal was found to be the initial step in erosion of the alloys and was responsible for most of the material loss during the incubation period. During steady state erosion both cobalt and WC grains were removed.

3. Erosion rate during the steady state was considered a better comparative measure of cavitation erosion than 5 hour volume loss.

4. The total strain accommodated by transformation of the binder increased with increasing binder content, thus improving the erosion resistance of high cobalt content alloys. The erosion is controlled by the binder for high binder content alloys.

5. For low binder content alloys the erosion is controlled by the strength and rigidity of the WC skeleton.

6. Corrosion was found to occur, but played a negligible role in the cavitation erosion.

REFERENCES

1. ALMOND E.A. and ROEBUCK B.,High Temperature and High Pressures vol 14, 1982, pp. 143-154.

2. ANTONY K.C. and SILENCE W.L., Proc. 5th Int. Conf. on Erosion by Liquid and Solid Impact, Cambridge, England, Sept 1979, pp.67-71.

3. BALL A. and PATERSON A.W., Proc. Int. Conf. in Recent Developments in Special Steels and Hard Metals, Rhodes Island, 1985, pp. 377-391.

4. BELL J.F.W. and SHARP J.C.K., Rev. Int Htes. Tem. et Refract., vol.12, no.1, 1975, pp. 40-43.

5. CHERMANT J.L. and OSTERSTOCK F., Powder Metallurgy International, vol. 11, no.3, 1979, pp. 106-109.

6. CHERMANT J.L., IOST A. and OSTERSTOCK F., Proc. British Ceramic Society, 1975, pp. 197-209.

7. CONRAD H., SHIN Y. and SARGENT G.A.,Proc. Int. Conf. in Recent Developments in Special Steels and Hard Metals, Pretoria, South Africa, 1982, pp. 423-429.

8. DAWIHL W. and FRISCH B., Cobalt, vol. 22, 1964, pp. 22-30.

9. DOI H., FUJIWARA Y., MIYAKE K. and OOSAWA Y., Met. Trans., vol 1, 1970, pp. 1417-1425.

10. EVANS A.G. and CHARLES E.A., Journal of the Americal Ceramic Society, vol.59, 1976, pp.371-372.

11. EXNER H.E., Int. Metals Review, no.4,1979, pp. 149-173.

12. EXNER H.E.and GURLAND J., Powder Metallurgy, vol. 13, no. 25, 1970, pp.13-31

13. EXNER H.E., PICKENS J.R. and GURLAND J., Met. Trans., vol 9A, 1978, pp. 736-738.

14. GOULD G.C., Proc. 3rd Int. Conf. on Rain Erosion, Farnborough, England, 1970, p. 881; cited in ref. 32, p. 289.

15. GURLAND J. and PARIKH M., Fracture, vol.2, 1972, ed. H. Lebowitz, pp. 841-878.

16. HEATHCOCK C.J., Ph.D. Thesis, UCT, 1980.

17. HIBBS M.K. and SINCLAIR R., Acta Met., vol. 29, 1981, pp. 1645-1654.

18. KARIMI and MARTIN J.L., Int. Metals Review, vol. 31, no.1, 1986, pp. 1-26.

19. KNAPP R.T., DAILY J.W. and HAMMITT F.G., "Cavitation", McGraw-Hill Book Co., New York, 1970.

20. LARSEN-BADSE J., Journal of Metals, 1983, pp. 35-42.

21. LAUGIER M.T., Journal of Mat. Sci. Letters, vol.4, 1985, pp. 207-210.

22. LEE H.C. and GURLAND J., Mat. Sci. and Eng., vol. 33, 1978, pp. 125-139.

23. LEUTH R., Fracture Mechanics of Ceramics, vol. 2, 1974, pp. 365-377.

24. LUYCKX S.B., Acta Met., vol. 16, 1968, pp. 535-544.

25. LUYCKX S.B., Acta Met., vol. 16, 1970, pp. 233-236.

26. MURRAY M.J., Proc. Royal Society, London, A356, 1977, pp. 438-508.

27 NIIHARA K., MORENA R. and HASSELMAN D.P.H., Journal of Mat. Sci. Letters, vol.1, 1982, pp. 13-16.

28. PENNEFATHER R.C., M.Sc Thesis, UCT, 1986.

29. PETERS C.T., Journal of Mat. Sci. vol. 14, 1979. pp. 1619-1623.

30. PETERS C.T. and COOPER R., Planseeberichte fur Pulvermetallurgie, vol. 26, 1978, pp. 181-190.

31. PLESSET M.S. and ELLIS A.T., Met. Trans. vol. 77, 1955, pp. 1055-1064.

32. PREECE C.M., Treatise on Materials Science and Technology (Erosion), vol. 16, Academic Press, 1979.

33. PRECCE C.M. and MACMILLAN N.H., Annual Review of Materials Science, vol. 7, 1977, pp. 95-121.

34. RAO B.C.S. and BUCKLEY D.H., Trans. ASLE, vol.29, 1985, pp. 473-480.

35. SHETTY D.K. and WRIGHT E.G., Journal of Mat. Sci. Letters, vol.5, 1986, pp. 365-368.

36. SHETTY D.K., WRIGHT I.G. and STROPKI J.T., Trans ASLE, vol. 28, 1984, pp. 123-133.

37. VAIDYA S. and PREECE C.M., Met. Trans., vol 9A, 1978, pp. 299-307.

38 VYAS B. and PREECE C.M., ASTM STP 567, 1973, pp. 77.

39. VYAS B. and PREECE C.M., Journal of Applied Physics, vol. 47, 1976, p. 5133.

40. VYAS B. and PREECE C.M., Met. Trans., vol 8A, 1977, pp. 915-923.

41. WOODFORD D.A, Met. Trans., vol. 3, 1972, pp. 77.

42. WRIGHT I. G., SHETTY D.K. and CLAUER A.H., Proc. 6th Int. Conf. on Erosion by Liquid and Solid Impact, 1983, pp. 63.1-63.8.

43. ZHOU Y. and HAMMITT F.G., Wear, vol. 86, 1983, pp. 299-313.

APPENDIX 1

DETERMINATION OF YOUNGS MODULUS USING THE IN-PLANE RESONANCES OF THIN DISKS

The two distortion resonances used in this study were the (1,3) and the (1,R). As Poisson's ratio (P) increases, the frequency of the (1,R) mode, F_{1R}, increases, while F_{13} decreases. Thus P can be calculated directly from the frequency ratio:

$$R1 = F_{1R}/F_{13} - 1 \qquad (1)$$

$$P = S + A(R1-R) \qquad (2)$$

where S = 0.2, A = 1.2077 and R = -0.12535

The theoretical analysis gives an eigen value, K, for each mode. K_{13} is obtained using P from equation (2):

$$K_{13} = K - 1.35(P-S) \qquad (3)$$

where K = 2.269 and S = 0.2

Using the eigen value calculated in equation (3) and F_{13}, the plate velocity, C_p, is calculated:

$$C_p = dF_{13}/K_{13} \qquad (4)$$

where d is the disk diameter.

From the plate velocity, the rod velocity, C_1, and hence the Youngs modulus can be obtained using:

$$C_1 = C_p(1-P^2)^{1/2} \qquad (5)$$

and $$E = C_1^2 p \qquad (6)$$

where p is the density.

These calculations were done using the following computer program on a Hewlett Packard 87 computer.

The computer program used to calculate Youngs modulus:

```
10   PRINTER IS 706,80
20   CLEAR
30   DISP "Number of Samples?"
40   INPUT N
50   PRINT "GRADE";TAB(10);"DENSITY";TAB(22);"SIGMA";TAB(32);"F/K";TAB(42);"E"
60   PRINT TAB(11);"g/cm3";TAB(41);"GPa"
70   PRINT "-------------------------------------------"
80   PRINT
85   I=0
90   FOR I=1 TO N
100  CLEAR
110  DISP "ENTER GRADE"
120  INPUT A$
130  DISP "ENTER F(1,3) in kHz"
140  INPUT F1
150  DISP "ENTER F(1,R) in kHz"
160  INPUT F2
170  DISP "ENTER DENSITY (g/cm3)"
180  INPUT G
190  DISP "ENTER DIAMETER (mm)"
200  INPUT D
210  S=.2
220  A=1.2077
230  R=-.12535
240  K=2.269
250  R1=F2/F1-1
260  P=S+A*(R1-R)
270  K1=K-1.35*(P-S)
280  K2=F1/K1
290  C1=PI*D*K2
300  C2=C1*SQR(1-P^2)
310  E=C2^2*G/1000000
330  PRINT USING 340 ; A$;G;P;K2;E
340  IMAGE X,3A,5X,2D.2D,6,Z.3D,4X,3D.D
350  NEXT I
360  END
```